NASA Technical Memorandum 106990
AIAA–96–1277

Layerwise Finite Elements for Smart Piezoceramic Composite Plates in Thermal Environments

Ho-Jun Lee
Lewis Research Center
Cleveland, Ohio

and

Dimitris A. Saravanos
Ohio Aerospace Institute
Cleveland, Ohio

Prepared for the
37th Structures, Structural Dynamics, and Materials Conference and Exhibit
cosponsored by AIAA, ASME, ASCE, AHS, and ASC
Salt Lake City, Utah, April 15–17, 1996

National Aeronautics and
Space Administration

LAYERWISE FINITE ELEMENTS FOR SMART PIEZOCERAMIC COMPOSITE PLATES IN THERMAL ENVIRONMENTS

Ho-Jun Lee
National Aeronautics and Space Administration
Lewis Research Center
Cleveland, Ohio 44135

and

Dimitris A. Saravanos*
Ohio Aerospace Institute
Brook Park, Ohio 44142

ABSTRACT

Analytical formulations are presented which account for the coupled mechanical, electrical, and thermal response of piezoelectric composite laminates and plate structures. A layerwise theory is formulated with the inherent capability to explicitly model the active and sensory response of piezoelectric composite plates having arbitrary laminate configurations in thermal environments. Finite element equations are derived and implemented for a bilinear 4-noded plate element. Application cases demonstrate the capability to manage thermally induced bending and twisting deformations in symmetric and antisymmetric composite plates with piezoelectric actuators, and show the corresponding electrical response of distributed piezoelectric sensors. Finally, the resultant stresses in the thermal piezoelectric composite laminates are investigated.

INTRODUCTION

The development of piezoelectric composite materials offers great potential for use in advanced aerospace structural applications. By taking advantage of the direct and converse piezoelectric effects, piezoelectric composite structures can combine the traditional performance advantages of composite laminates along with the inherent capability of piezoelectric materials to adapt to their current environment. Extensive development of analytical methods for modeling the isothermal behavior of piezoelectric composite structures has been reported. The initial application of piezoelectric materials as actuators involved the vibration control of beams[1-2] and lead to the development of simplified models for beams. Advances in theoretical models lead to both a piezoelectric plate theory[3-4] and a piezoelectric thin shell theory[5], based on the assumptions of classical plate and shell theory, respectively. Subsequent developments led to a variety of finite element formulations for beam[6-7], plate[8-9], shell[10-13], and solid[14-15] elements.

---

* NASA Resident Research Associate at Lewis Research Center

Additional approaches have been reported on refined piezoelectric laminate theories which account for the limitations of classical laminate plate theory (CLPT)[16-17]. These approaches, called discrete layer theories, provide a generalization of both the classical and higher order theories, and allow separate displacement fields to be assumed in each layer of the laminate. A discrete layer beam theory for analyzing piezoelectric beams was first reported by Robbins and Reddy[6] using an induced strain approach to approximate the piezoelectric effect. Heyliger and Saravanos[18-20] subsequently presented discrete layer beam and plate theories explicitly accounting for the coupled equations of piezoelectricity, which have lead to generalized multi-field finite element formulations.

All of the previously described works neglect the implication of thermal effects on both the active and sensory response of piezoelectric structures, even though an area where piezoelectric materials may provide dramatic advantages is in the development of smart thermal structures with the capability to sense and actively compensate for thermally induced deformations. Thermal loads will typically affect the response of smart piezoelectric laminates with four distinct physical mechanisms: (1) induction of thermal strains due to coefficient of thermal expansion mismatch between the various composite plies and piezoelectric layers, (2) pyroelectric effects on the electric displacement of the piezoelectric material, (3) changes in the piezoelectric and dielectric properties of the piezoelectric materials, and (4) changes in the elastic properties of the composite and piezoelectric materials. Only limited research has been reported in this area. Two-dimensional thermopiezoelectric equations for plates were formulated by Mindlin[21]. A thermopiezoelectric laminate plate theory and a thin shell theory, based on classical assumptions, were reported by Tauchert[22] and Tzou and Howard[23], respectively. Subsequent developments in thermopiezoelectric finite elements include a beam element by Rao and Sunar[24,25], a shell element using induced strain approximations for the electric and thermal effects by Chandrashekhara and Kolli[26], a solid element using an induced thermal strain approach by Ha et al.[27], and a thin solid element by Tzou and Ye[28-29]. Many of these previous approaches utilize simplified laminate assumptions and neglect the coupling effects existing in thermopiezoelectric laminates. To remedy these limitations, discrete layer approaches for smart thermopiezoelectric beam structures were reported by Lee and Saravanos[30-32].

This paper presents the extension of the discrete layer mechanics[30-32] for the analysis of smart thermopiezoelectric plate structures and addresses the problem of active thermal distortion management with smart piezoelectric plates. The mechanics account for the coupled mechanical, electrical, and thermal response of piezoelectric laminates at the material level through the thermo-piezoelectric constitutive equations. The displacements, electric potential and temperature are assumed to be layerwise (piecewise continuous) fields through the laminate thickness. This layerwise generalization provides the capability to capture the locally induced piezoelectric effects, which leads to increased accuracy in laminate stress predictions (especially for thick laminates, and/or laminates with strong thermal and elastic inhomogeneities through-the-thickness). A corresponding finite element formulation is presented using the layerwise laminate theory and a 4-noded plate element is developed. Numerical studies demonstrate the capability to actively manage thermally induced twisting and bending deformations in piezoelectric symmetric and antisymmetric composite plates subjected to thermal gradients, as well as examining the corresponding voltage response of piezoelectric sensors and the resulting intralaminar and interlaminar stresses in active thermo-

piezoelectric plates.

GOVERNING MATERIAL EQUATIONS

This section outlines the governing equations for thermopiezoelectric materials. The mechanical response is represented by the stress-equilibrium equation,

$$\sigma_{ij,j} + f_i = \rho\, \ddot{u}_i \tag{1}$$

where σ_{ij}, f_i, ρ, u_i are the stress, body force per unit volume, density, and displacement, respectively; with i, j = 1, 2, 3. Maxwell's equation for the conservation of electric displacements D_i is

$$D_{i,i} = 0 \tag{2}$$

The constitutive equations for a thermopiezoelectric material[33] employing standard contracted notation are

$$S_\alpha = s^{E,T}_{\alpha\beta}(T)\, \sigma_\beta + d^{T}_{\alpha m}(T)\, E_m + \alpha^{E,T}_{\alpha}(T)\, \theta \tag{3}$$

$$D_m = d^{T}_{m\alpha}(T)\, \sigma_\alpha + \epsilon^{\sigma,T}_{mk}(T)\, E_k + p^{\sigma,T}_{m}(T)\, \theta \tag{4}$$

or in semi-inverted form

$$\sigma_\alpha = C^{E,T}_{\alpha\beta}(T)\, S_\beta - e^{T}_{\alpha m}(T)\, E_m - \lambda^{E,T}_{\alpha}(T)\, \theta \tag{5}$$

$$D_m = e^{T}_{m\alpha}(T)\, S_\alpha + \epsilon^{S,T}_{mk}(T)\, E_k + p^{S,T}_{m}(T)\, \theta \tag{6}$$

where S_α represents the strain tensor; E_m the electric field vector; $\theta = \Delta T = T - T_o$ is the temperature difference from the current temperature T and the thermally stress free reference temperature T_o; and

$$\begin{aligned} e^{T}_{\alpha m}(T) &= C^{E,T}_{\alpha\beta}(T)\, d^{T}_{\beta m}(T)\, E_m \\ \lambda^{E,T}_{\alpha}(T) &= C^{E,T}_{\alpha\beta}(T)\, \alpha^{E,T}_{\beta}(T) \\ \epsilon^{S,T}_{mk}(T) &= \epsilon^{\sigma,T}_{mk}(T) - d^{T}_{m\alpha}(T)\, e^{T}_{\alpha k}(T) \\ p^{S,T}_{m}(T) &= p^{\sigma,T}_{m}(T) - d^{T}_{m\alpha}(T)\, \lambda^{E,T}_{\alpha}(T) \end{aligned} \tag{7}$$

where $C_{\alpha\beta}$ and $s_{\alpha\beta}$ are the elastic stiffness and compliance tensors; $d_{\alpha m}$ and $e_{\alpha m}$ are the different forms

of the piezoelectric tensor due to inversion; ϵ_{mk} is the electric permittivity tensor; α_α and λ_α are the different forms of the coefficient of thermal expansion due to inversion; p_m is the pyroelectric constant; superscripts E, σ, S, and T, represent constant voltage, constant stress, constant strain, and constant temperature conditions, respectively; α, β = 1, ...,6; and k, m = 1, 2, 3.

The small deformation strain-displacement relations are

$$S_{ij} = \frac{1}{2}\,(u_{i,j} + u_{j,i}) \tag{8}$$

and the electric field vector is related to the electric potential ϕ by

$$E_i = -\,\phi_{,i} \tag{9}$$

Through use of the divergence theorem and neglecting body forces, Eqs. (1) and (2) can be expressed in an equivalent variational form as

$$\int_V (\rho\ \ddot{u}_i\ \delta u_i + \sigma_{ij}\ \delta S_{ij} - D_i\ \delta E_i)\ dV = \int_\Gamma t_i\ \delta u_i\ d\Gamma + \int_{\Gamma_p} q\ \delta\phi\ d\Gamma \tag{10}$$

where t_i are the surface tractions applied on the bounding surface Γ; q is the electrical charge applied on the surface Γ_p of the piezoelectric material; and V represents the whole volume including both composite and piezoelectric materials.

DISCRETE LAYER LAMINATE THEORY

A discrete layer laminate theory for thermopiezoelectric composite plates is formulated by introducing the following piecewise continuous approximations for the state variables

$$u(x,y,z,t) = \sum_{j=1}^{N} U^j(x,y,t)\ \psi^j(z) \tag{11}$$

$$v(x,y,z,t) = \sum_{j=1}^{N} V^j(x,y,t)\ \psi^j(z) \tag{12}$$

$$w(x,y,z,t) = W^o(x,y,t) \tag{13}$$

$$\phi(x,y,z,t) = \sum_{j=1}^{N} \phi^j(x,y,t)\ \psi^j(z) \tag{14}$$

$$\theta(z,t) = \sum_{j=1}^{N} \theta^j(t)\ \psi^j(z) \tag{15}$$

where N is the number of interpolation functions ψ^j. Currently, ψ^j is represented using linear Lagrangian interpolation functions, although in general any order of interpolation functions can be used. U^j, V^j, W^o, ϕ^j, and θ^j are the generalized laminate state variables, in which a constant through-the-thickness displacement is assumed for w. This assumption of constant through-the-thickness displacement leads to a simplified set of constitutive equations, derived from Eqs. (3)-(6), shown in Appendix A.

By substituting Eqs. (5)-(9) and (11)-(15) into Eq. (10) and integrating through-the-thickness, the following variational form is obtained

$$
\begin{aligned}
&\sum_{k=1}^{N}\sum_{m=1}^{N}\int_{A}(P_{11}^{km}\ddot{u}^{m}\delta u^{k}+P_{22}^{km}\ddot{v}^{m}\delta v^{k})dA+\int_{A}P_{33}\ddot{w}\delta w dA\\
&\sum_{k=1}^{N}\sum_{m=1}^{N}\int_{A}\{A_{11}^{km}u_{x}^{m}\delta u_{x}^{k}+A_{12}^{km}(u_{x}^{m}\delta v_{y}^{k}+v_{y}^{m}\delta u_{x}^{k})+\\
&A_{16}^{km}(u_{x}^{m}\delta u_{y}^{k}+u_{y}^{m}\delta u_{x}^{k}+u_{x}^{m}\delta v_{x}^{k}+v_{x}^{m}\delta u_{x}^{k})+A_{22}^{km}v_{y}^{m}\delta v_{y}^{k}+\\
&A_{26}^{km}(u_{y}^{m}\delta v_{y}^{k}+v_{y}^{m}\delta u_{y}^{k}+v_{x}^{m}\delta v_{y}^{k}+v_{y}^{m}\delta v_{x}^{k})+\\
&A_{66}^{km}(u_{y}^{m}\delta u_{y}^{k}+u_{y}^{m}\delta v_{x}^{k}+v_{x}^{m}\delta v_{x}^{k}+v_{x}^{m}\delta u_{y}^{k})\}dA+\\
&\sum_{m=1}^{N}\int_{A}\{B_{44}^{m}(v^{m}\delta w_{y}+w_{y}\delta v^{m})+B_{55}^{m}(u^{m}\delta w_{x}+w_{x}\delta u^{m})+\\
&B_{45}^{m}(u^{m}\delta w_{y}+v^{m}\delta w_{x}+w_{x}\delta v^{m}+w_{y}\delta u^{m})\}dA+\\
&\int_{A}\{\overline{C_{44}}w_{y}\delta w_{y}+\overline{C_{45}}(w_{x}\delta w_{y}+w_{y}\delta w_{x})+\overline{C_{55}}w_{x}\delta w_{x}\}dA\\
&\sum_{k=1}^{N}\sum_{m=1}^{N}\int_{A}\{D_{44}^{km}v^{m}\delta v^{k}+D_{45}^{km}(u^{m}\delta v^{k}+v^{m}\delta u^{k})+D_{55}^{km}u^{m}\delta u^{k}+\\
&E_{31}^{km}u_{x}^{m}\delta\phi^{k}+E_{32}^{km}(v_{y}^{m}\delta\phi^{k}+E_{36}^{km}(u_{y}^{m}\delta\phi^{k}+v_{x}^{m}\delta\phi^{k})+\\
&\overline{E_{31}^{km}}\phi^{m}\delta u_{x}^{k}+\overline{E_{32}^{km}}\phi^{m}\delta v_{y}^{k}+\overline{E_{36}^{km}}(\phi^{m}\delta u_{y}^{k}+\phi^{m}\delta v_{x}^{k})\\
&-G_{11}^{km}\phi_{x}^{m}\delta\phi_{x}^{k}-G_{22}^{km}\phi_{y}^{m}\delta\phi_{y}^{k}-G_{33}^{km}\phi^{m}\delta\phi^{k}\}dA\\
&\sum_{m=1}^{N}\int_{A}\{-f_{1,th}^{m}\delta u_{x}^{m}-f_{2,th}^{m}\delta v_{y}^{m}+q_{1,th}^{m}\delta\phi_{x}^{m}+q_{2,th}^{m}\delta\phi_{y}^{m}+q_{3,th}^{m}\delta\phi^{m}\}dA\\
&=\int_{\Gamma}t_{i}\,\delta u_{i}d\Gamma+\int_{\Gamma_{p}}q\,\delta\phi d\Gamma
\end{aligned}
\tag{16}
$$

in which the dependence of the z-coordinate has been separated into the generalized density matrix [P], the stiffness matrices [A], [B], [C], [D], the piezoelectric matrix [E], the dielectric permittivity matrix [G], and the thermal force matrices [$f_{,th}$] and [$q_{,th}$]. These generalized laminate matrices are listed in Appendix B.

FINITE ELEMENT FORMULATION

The finite element formulation for a composite piezoelectric plate is obtained by incorporating additional local in-plane approximations to the state variables

$$
u(x,y,z,t)=\sum_{i=1}^{M}\sum_{j=1}^{N}U^{ji}(t)\,R^{i}(x,y)\,\psi^{j}(z) \tag{17}
$$

$$v(x,y,z,t) = \sum_{i=1}^{M} \sum_{j=1}^{N} V^{ji}(t)\, R^{i}(x,y)\, \psi^{j}(z) \tag{18}$$

$$w(x,y,z,t) = \sum_{i=1}^{M} W^{oi}(t)\, R^{i}(x,y) \tag{19}$$

$$\phi(x,y,z,t) = \sum_{i=1}^{M} \sum_{j=1}^{N} \phi^{ji}(t)\, R^{i}(x,y)\, \psi^{j}(z) \tag{20}$$

where M is the number of in-plane shape functions R. Currently, R is represented using bilinear Lagrangian interpolation functions.

By combining Eqs. (16)-(20), the following finite element matrix formulation is obtained for the case of a constant through-the-thickness displacement plate

$$\begin{bmatrix} [M_{11}] & 0 & 0 & 0 \\ 0 & [M_{22}] & 0 & 0 \\ 0 & 0 & [M_{33}] & 0 \\ 0 & 0 & 0 & 0 \end{bmatrix} \begin{Bmatrix} \{\ddot{U}\} \\ \{\ddot{V}\} \\ \{\ddot{W}\} \\ \{\Phi\} \end{Bmatrix} + \begin{bmatrix} [K_{11}] & [K_{12}] & [K_{13}] & [K_{14}] \\ [K_{21}] & [K_{22}] & [K_{23}] & [K_{24}] \\ [K_{31}] & [K_{32}] & [K_{33}] & 0 \\ [K_{41}] & [K_{42}] & 0 & [K_{44}] \end{bmatrix} \begin{Bmatrix} \{U\} \\ \{V\} \\ \{W\} \\ \{\Phi\} \end{Bmatrix} = \begin{Bmatrix} \{F_1\} \\ \{F_2\} \\ \{F_3\} \\ \{Q\} \end{Bmatrix} + \begin{Bmatrix} \{F_{1,th}\} \\ \{F_{2,th}\} \\ \{F_{3,th}\} \\ \{Q_{th}\} \end{Bmatrix} \tag{21}$$

where the elements of the submatrices above are calculated in accordance with the generalized discrete layer laminate matrices defined previously in Appendix B. The finite element submatrices for the mass, stiffness, external force, and thermal force are included in Appendix C.

The coupled finite element formulation can also be expressed in a compact form with the electric potential partitioned into active and sensory components such that

$$\begin{bmatrix} [M_{uu}] & 0 \\ 0 & 0 \end{bmatrix} \begin{Bmatrix} \{\ddot{U}\} \\ \{\Phi^s\} \end{Bmatrix} + \begin{bmatrix} [K_{uu}] & [K_{u\phi}^{ss}] \\ [K_{\phi u}^{ss}] & [K_{\phi\phi}^{ss}] \end{bmatrix} \begin{Bmatrix} \{U\} \\ \{\Phi^s\} \end{Bmatrix} = \begin{Bmatrix} \{F\} + \{F_{th}\} - [K_{u\phi}^{sa}]\{\Phi^a\} \\ \{Q^s\} + \{Q_{th}^s\} - [K_{\phi\phi}^{sa}]\{\Phi^a\} \end{Bmatrix} \tag{22}$$

where the superscripts s and a indicate the partitioned electric potential vectors in either sensory or active configurations, respectively. This form has the advantage of positioning the unknown variables (displacements and sensory electric potentials) in the left-hand terms, while the known quantities (mechanical loads, thermal loads, electric charges, and active voltages) are included in the right-hand terms.

The partitioned finite element formulation of Eq. (22) can be easily uncoupled into the following independent equations for the structural displacements

$$[M_{uu}]\{\ddot{U}\} + ([K_{uu}] - [K_{u\phi}^{ss}][K_{\phi\phi}^{ss}]^{-1}[K_{\phi u}^{ss}])\{U\} =$$
$$\{F\} + \{F_{th}\} + ([K_{u\phi}^{ss}][K_{\phi\phi}^{ss}]^{-1}[K_{\phi\phi}^{sa}] - [K_{u\phi}^{sa}])\{\Phi^a\} \tag{23}$$

and the sensory electric potentials

$$\{\Phi^s\} = -[K_{\phi\phi}^{ss}]^{-1}([K_{\phi u}^{ss}]\{U\} + [K_{\phi\phi}^{sa}]\{\Phi^a\} - \{Q^s\} - \{Q_{th}^s\}) \tag{24}$$

APPLICATIONS

Simply Supported $[0/\pm45]_s$ Graphite/Epoxy Plate with Discrete Piezoceramic Patches

This case study is a problem of active thermal distortion management, examined previously by Ha et al.[27], of a 37.2 cm x 22.8 cm x 0.75 mm $[0/\pm45]_s$ graphite/epoxy plate with fifteen 6.0 cm x 6.0 cm x 0.13 mm piezoceramic patches uniformly attached to each top and bottom surface (see Figure 1). A thermal gradient (50°C on the top surface and −50°C on the bottom surface) is applied to the plate. Figure 1 illustrates the geometry and finite element mesh of the plate. The plate is simply supported along the two edges parallel to the y-axis and is free on the two edges parallel to the x-axis. The material properties used for both the composite and piezoceramic materials are listed in Table I. The objective was to apply increasing active voltages on both the top and bottom piezoceramic patches to minimize the out-of-plane deflection induced by the thermal gradient. Additional studies investigate the sensory response of the piezoceramic patches operating in a combined sensor and actuator mode, as well as the development of local stresses in the plate with all piezoceramic patches operating as actuators.

Active Thermal Distortion Control. The resulting bending deformation with 0 Volts applied on both surfaces of the piezoceramic patches is shown in Figure 2(a). Through application of increasing active voltages in the piezoceramic patches, the thermally induced deformation of the plate can be gradually eliminated. Figures 2(b) and 2(c) demonstrate the reduction in the out-of-plane deflection achieved by applying active voltages of 34 V and 70 V, respectively. The active voltage is applied on the outer surface of each of the piezoceramic patches, while the inner surface (i.e. the surface in contact with the plate) is grounded. The same voltages are applied to both the upper and lower piezoceramic patches. A comparison of centerline deflections (along y/b=0.5) predicted by Ha et al.[27] and by the current formulation, along with the corresponding active voltages, is shown in Figure 3. In order to obtain the same reduction in centerline deflection as Ha et al., slightly higher active voltages were applied using the current method (34 and 70 Volts, as compared to 31 and 61 Volts for Ha et al.). These differences between the two analyses are most likely due to the different formulations and elements used. Ha et al. uses a three-dimensional brick element in their analysis, while the current method utilizes a layerwise plate theory and

element which assumes a constant through-the-thickness displacement w. This use of a plate theory neglects certain material properties that Ha et al's. analysis considers (specifically C_{13}, C_{23}, C_{33}, d_{24}, d_{33}, and α_{33}). Another difference is the explicit incorporation of thermal terms in the constitutive equations of the current formulation, which are neglected in Ha et al's. analysis.

Sensory Voltages. Besides the fully active configurations previously studied (active potentials applied to all piezoceramic patches), other electric configurations yielding combinations of piezoceramic sensors and actuators are sometimes more desirable. The current formulation has the capability to explicitly predict sensory voltages. These sensory capabilities are demonstrated on an active/sensory configuration of the $[0/\pm45]_s$ graphite/epoxy plate. The upper layer of piezoceramic patches are used as sensors, while the bottom layer of patches are maintained as actuators. In the sensory application, the inner surface of each piezoceramic patch is grounded while the outer surface is free to develop a sensory electric potential. Figures 4(a)-4(c) show the sensory voltages that develop on the upper piezoceramic patches upon combined application of a thermal gradient with active voltages of 0, 34, and 70 Volts on the lower piezoelectric patches, respectively. Generally, there is a reduction in the sensory voltage values which corresponds to the reduction in out-of-plane deflection with increasing active voltages. However, additional contributions remain from local stresses and pyroelectric effects. In actual applications, these measured sensory voltages will be used in a control loop to provide the inferred feedback essential for monitoring and actively controlling the thermal distortions.

Local Stresses. The development of high local stress fields in a thermopiezoelectric laminate from the mismatch in induced thermal and piezoelectric strains is also an area of primary concern, since it will affect the integrity of these structures. As stated previously, one strong advantage of the layerwise approach is the accurate calculation of intralaminar in-plane stresses and interlaminar shear stresses in piezoelectric composite laminates (Heyliger and Saravanos[18-20]). Consequently, this section presents the stress fields for the $[0/\pm45]_s$ graphite/epoxy plate problem with both piezoceramic layers used as actuators. In these studies, a continuous piezoceramic layer is used instead of many distributed piezoceramic patches to eliminate the need for a highly refined mesh. The stresses are nondimensionalized using an equivalent laminate moduli defined as

$$<E_{Lij},G_{Lij}>=\frac{1}{h}\int_0^h <E_{ij},G_{ij}>\,dz$$

Figures 5(a)-5(c) show the variation of normal stresses (σ_{xx}, σ_{yy}) and in-plane shear stress (σ_{xy}) through-the-thickness at x/a=0.5 and y/b=0.4 with the different applied voltages, while Figures 5(d)-5(e) show the variation of interlaminar shear stresses (σ_{xz}, σ_{yz}) through-the-thickness near the free edge at x/a=0.9 and y/b=0.4. The normal stresses in Figures 5(a) and 5(b) increase as higher active voltages are applied reflecting the increase in piezoelectric strains, which indicates that one potential tradeoff for minimizing thermal distortions would be increased normal stresses. Thus, the stress state in thermopiezoelectric laminates (and particularly in the actuators) should be among the primary design considerations. The normal stresses can also be separated into individual components as shown in Figures 6(a) and 6(b) for the 70 V case (the shear stresses contain only an elastic component in the current study). The three components correspond to the three terms found on the right hand side of Eq. (5) and represent the individual stresses which are induced from the elastic, piezoelectric,

and thermal effects. This shows how the individual stress components are affecting the overall stress state of the plate.

Cantilevered $[45_3/-45_3]$ Graphite/Epoxy Plate with Discrete Piezoceramic Patches

A numerical study was also conducted on a $[45_3/-45_3]$ antisymmetric graphite/epoxy laminate with attached piezoceramic patches. The plate has the same geometry and material properties used in the previous section and is clamped along the x=0 edge, while the other three edges remain free. A thermal gradient (15°C on the top surface and -15°C on the bottom surface) is applied to the plate with 0 Volts applied on both surfaces of the piezoceramic patches. The objective of this study is to minimize, both individually and in combination, the thermally induced bending and twisting deformations through application of active voltages.

Active Thermal Distortion Control. Application of a 30°C thermal gradient, with all piezoceramic patches grounded, results in the combined bending and twisting deformation shown in Figure 7(a). Through application of active voltages of varying polarities in the piezoceramic patches, the bending and twisting deformations can be inhibited either individually or in combination. As demonstrated in the previous problem, the bending deformation can be managed through application of voltages which have the opposite polarity. By applying 40 V to both the top and bottom layers of piezoceramic patches, the bending deformation can be eliminated as shown in Figure 7(b). The twisting deformation remains unaffected and is now more apparent due to the removal of thermal bending. In a similar manner, the twisting deformation of the plate can be eliminated, without affecting the bending behavior as shown in Figure 7(c). This requires the application of voltages with the same polarities, specifically 145 V is applied to the top layer of piezoceramic patches, while -145 V is applied to the bottom layer of piezoceramic patches. Finally, in order to inhibit both the bending and twisting deformations simultaneously, the previous voltages are superposed. Thus, by applying 185 V on the upper and -105 V on the lower piezoceramic patches, all deformations in the plate can be compensated, as shown in Figure 7(d). These results demonstrate the potential of piezoelectric structures to selectively manage desired thermal distortions.

Sensory Voltages. The sensory capabilities of the current formulation are demonstrated on a combined active/sensory configuration of the $[45_3/-45_3]$ graphite/epoxy plate. The upper layer of piezoceramic patches are used as sensors, while the bottom layer of patches are maintained as actuators. Figure 8 shows the voltages that develop on the upper surface sensors upon combined application of a thermal gradient and 0 Volts on the lower piezoelectric actuators. These sensory voltages will provide the electric feedback required to monitor the state of deformation in the plate.

Local Stresses. This section presents the stress fields for the active $[45_3/-45_3]$ graphite/epoxy plate problem. As before, a continuous piezoceramic layer is used instead of many distributed piezoceramic patches to eliminate the need for a highly refined mesh in this study. Figures 9(a)-9(c) show the variation of normal stresses (σ_{xx}, σ_{yy}) and in-plane shear stress (σ_{xy}) through-the-thickness at x/a=0.5 and y/b=0.4 with the various applied voltages, while Figures 9(d)-9(e) show the variation of

interlaminar shear stresses (σ_{xz}, σ_{yz}) through-the-thickness near the free edge at x/a=0.9 and y/b=0.4. The normal stresses in Figures 9(a) and 9(b) indicate that similar high stress states arise from minimizing the twisting of the plate individually (145 V on top and -145 V on bottom layer) or simultaneously with bending (185 V on top and -105 V on bottom layer). In contrast, minimizing the bending behavior independently (40 V on both top and bottom layers) has little effect on the normal stresses. It is recalled that the twisting was compensated by taking advantage of the extension-twisting coupling in this laminate. The in-plane shear stress shown in Figure 9(c) indicates that regardless of the applied active voltage, high shear stresses will occur in the plate. The normal stresses can also be separated into the individual components as shown in Figures 10(a) and 10(b) for the case of combined active elimination of thermal twisting and bending (185 V applied on the upper piezoceramic patches and -105 V applied on the lower piezoceramic patches). The three components correspond to the three terms found on the right hand side of Eq. (5) and show the effect of the individual stresses on the overall stress state of the plate.

SUMMARY

Layerwise laminate and structural mechanics were described to model the coupled mechanical, electrical, and thermal behavior of smart piezoelectric composite laminates and plate structures. A finite element formulation and a bilinear 4-noded plate element were developed and encoded into prototype software. Thus, a necessary analytical and computational capability was developed to analyze the global and local response of smart piezoceramic plate structures operating in thermal environments.

The accuracy of the formulation was compared with previously published analytical results. Numerical studies were performed on symmetric $[0/\pm45]_s$ and antisymmetric $[45_3/-45_3]$ composite plates subject to thermal gradient with discrete piezoceramic patches attached on both surfaces, which demonstrated the capability to actively manage thermally induced bending and twisting deformations. The corresponding electric voltages developed at distributed piezoelectric sensors were also calculated. Finally, the severe stress fields through-the-thickness of the composite plates were predicted and the contributions of the thermal and piezoelectric components quantified. The numerical studies have indicated the significance of thermal effects on the performance of piezoelectric structures in extreme temperature environments and demonstrated the capabilities of the mechanics to accurately model such behavior.

REFERENCES

1 Bailey , T. and Hubbard, J.E., "Distributed Piezoelectric-Polymer Active Vibration Control of a Cantilever Beam," *J. Guidance*, Vol. 8, No. 5, 605-611, 1985.

2 Crawley, E.F. and de Luis, J., "Use of Piezoelectric Actuators as Elements of Intelligent Structures," *AIAA J.*, Vol. 25, No. 10, 1373-1385, 1987.

3 Lee, C.K., "Theory of Laminated Piezoelectric Plates for the Design of Distributed Sensors/Actuators. Part I: Governing Equations and Reciprocal Relationships," *J. Acoust. Soc. Amer.*, Vol 87, No. 3, 1144-1158, 1990.

4 Wang, B.-T. and Rogers, C.A., "Laminate Plate Theory for Spatially Distributed Induced Strain Actuators," *J. Comp. Mat.*, Vol. 25, 433-452, 1991.

5 Tzou, H.S. and Gadre, M., "Theoretical Analysis of a Multi-Layered Thin Shell Coupled with Piezoelectric Shell Actuators for Distributed Vibration Controls," *J. Sound Vib.*, Vol. 132, No. 3, 433-450, 1989.

6 Robbins, D.H. and Reddy, J.N., "Analysis of Piezoelectrically Actuated Beams Using a Layer-Wise Displacement Theory," *Comput. Struct.*, Vol. 41, No. 2, 265-279, 1991.

7 Shieh, R.C., "Governing Equations and Finite Element Methods for Multiaxial Piezoelectric Beam Sensors/Actuators," *AIAA J.*, Vol. 32, No.6, 1250-1258, 1994.

8 Hwang, W.-S. and Park, H.C., "Finite Element Modeling of Piezoelectric Sensors and Actuators," *AIAA J.*, Vol. 31, No. 5, 930-937, 1993.

9 Chandrashekhara, K. and Agarwal, A.N., "Active Vibration Control of Laminated Composite Plates Using Piezoelectric Devices: A Finite Element Approach," *J. Intel. Mat. Syst. Struct.*, Vol. 4, 496-508, 1993.

10 Lammering, R., "The Application of a Finite Shell Element for Composites Containing Piezoelectric Polymers in Vibration Control," *Comput. Struct.*, Vol. 41, No.5, 1101-1109, 1991.

11 Tzou, H.S. and Tseng, C.I., "Distributed Dynamic Identification and Controls of Flexible Shells: Theory and Finite Element Development," *Proceedings of the 31st Structures, Structural Dynamics, and Materials Conference*, Long Beach, CA, 2265-2273, 1990.

12 Tzou, H.S. and Tseng, C.I., "Distributed Piezoelectric Sensor/Actuator Design for Dynamic Measurement/Control of Distributed Parameter Systems: A Piezoelectric Finite Element Approach," *J. Sound Vib.*, Vol. 138, No. 1, 17-34, 1990.

13 Tzou, H.S. and Ye, R., "Analysis of Laminated Piezoelectric Shell Systems with C^0 Piezoelectric Triangle Finite Elements," *Proceedings of Adaptive Structures and Composite Materials: Analysis and Application*, ASME, AD-Vol. 45, 113-124, 1994.

14 Allik, H. and Hughes, T.J.R., "Finite Element Method for Piezoelectric Vibration," *Int. J. Numer. Method Eng.*, Vol. 2, 151-157, 1970.

15 Ha, S.K. and Chang, F.-K., "Finite Element Modeling of the Response of Laminated Composites with Distributed Piezoelectric Actuators," *Proceedings of the 31st Structures, Structural Dynamics, and Materials Conference*, Long Beach, CA, 2323-2330, 1990.

16 Reddy, J.N., "A Generalization of Two-Dimensional Theories of Laminated Composite Plates," *Commun. Appl. Numer. Methods*, Vol. 3, 173-180, 1987.

17 Reddy, J.N., "An Evaluation of Equivalent Single-Layer and Layerwise Theories of Composite Laminates," *Compos. Struct.*, Vol. 25, 21-35, 1993.

18 Heyliger, P.R. and Saravanos, D.A., "On Discrete-Layer Mechanics for Health-Monitoring Applications in Sensory/Active Composite Laminates," *Proceedings of ASME Winter Annual Meeting*, New Orleans, LA, 1993.

19 Heyliger, P.R., Ramirez, G., and Saravanos, D.A., "Coupled Discrete-Layer Finite Elements for Laminated Piezoelectric Plates," *Commun. Numer. Methods Eng.*, Vol. 10, 971-981, 1994.

20 Saravanos, D.A. and Heyliger, P.R., "Layerwise Mechanics and Finite Element for the Dynamic Analysis of Piezoelectric Composite Plates," *Int. J. Solids Struct.*, in press.

21 Mindlin, R.D., "Equations of High Frequency Vibrations of Thermopiezoelectric Crystal Plates," *Int. J. Solids Struct.*, Vol. 10, 625-632, 1974.

22 Tauchert, T.R., "Piezothermoelastic Behavior of a Laminated Plate," *J. Thermal Stresses*, Vol. 15, 25-37, 1992.

23 Tzou, H.S. and Howard, R.V., "A Piezothermoelastic Thin Shell Theory Applied to Active Structures," *J. Vib. Acoust.*, Vol. 116, 295-302 , 1994.

24 Sunar, M. and Rao, S.S., "Distributed Thermopiezoelectric Sensors and Actuators in Structural Design," *Proceedings of the 33rd Structures, Structural Dynamics, and Materials Conference*, Dallas, TX, 890-895, 1992.

25 Rao, S.S. and Sunar, M., "Analysis of Distributed Thermopiezoelectric Sensors and Actuators in Advanced Intelligent Structures," *AIAA J.*, Vol. 31, No. 7, 1280-1286, 1993.

26 Chandrashekhara, K. and Kolli, M., "Thermally Induced Vibration of Adaptive Doubly Curved Composite Shells with Piezoelectric Devices," *Proceedings of the 36th Structures, Structural Dynamics, and Materials Conference*, New Orleans, LA, 1628-1636, 1995.

27 Ha, S.K., Keilers, C., and Chang, F.-K., "Finite Element Analysis of Composite Structures Containing Distributed Piezoceramic Sensors and Actuators," *AIAA J.*, Vol. 30, No. 3, 772-780, 1992.

28 Tzou, H.S. and Ye, R., "Piezothermoelasticity and Precision Control of Piezoelectric Systems: Theory and Finite Element Analysis," *J. Vib. Acoust.*, Vol. 116, 489-495, 1994.

29 Tzou, H.S. and Ye, R., "Pyroelectric and Thermal Strain Effects of Piezoelectric (PVDF and PZT) Devices," *Proceedings of Adaptive Structures and Composite Materials: Analysis and Application*, ASME, AD-Vol. 45, 125-132, 1994.

30 Lee, H.-J. and Saravanos, D.A., "On The Response of Smart Piezoelectric Composite Structures in Thermal Environments," *Proceedings of the 36th Structures, Structural Dynamics, and Materials Conference*, New Orleans, LA, pp. 2876-2885, 1995.

31 Lee, H.-J. and Saravanos, D.A., "A Coupled Layerwise Analysis of the Thermopiezoelectric Response of Smart Composite Beams," *NASA Technical Memorandum 106889*, 1995.

32 Lee, H.-J. and Saravanos, D.A., "Coupled Layerwise Analysis of Thermopiezoelectric Composite Beams," *AIAA J.* , in press.

33 Nye, J.F., *Physical Properties of Crystals*, The Clarendon Press, Oxford, 1964.

TABLE I: Material properties of piezoceramic (PZT G1195N) and graphite/epoxy (T300/976) composite[27]

	Piezoceramic	Graphite/Epoxy
Elastic Moduli (GPa):		
E_{11}	63.0	150.0
E_{22}	63.0	9.0
E_{33}	63.0	9.0
Poisson's Ratio:		
υ_{12}	0.3	0.3
υ_{23}	0.3	0.3
υ_{31}	0.3	0.3
Shear Moduli (GPa):		
G_{12}	24.2	7.10
G_{23}	24.2	2.50
G_{31}	24.2	7.10
Density (kg/m^3):		
ρ	7600.	1600.
Piezoelectric Charge Constant (pm/V) :		
d_{14}	0.	0.
d_{15}	0.	0.
d_{24}	0.	0.
d_{25}	0.	0.
d_{31}	254.	0.
d_{32}	254.	0.
d_{36}	0.	0.
Electric Permittivity (nf/m):		
ϵ_{11}	15.3	0.
ϵ_{22}	15.3	0.
ϵ_{33}	15.0	0.
Thermal Expansion Coefficient (μm/m °C):		
α_{11}	0.9	1.1
α_{22}	0.9	25.2
Reference Temperature, T_0, (°C):	20.	20.

Appendix A:

Thermopiezoelectric Constitutive Equations for a Constant Through-the-Thickness Displacement Plate

The simplified constitutive equations for a constant through-the-thickness displacement plate are

$$\begin{Bmatrix} S_1 \\ S_2 \\ S_4 \\ S_5 \\ S_6 \end{Bmatrix} = \begin{bmatrix} s_{11} & s_{12} & 0 & 0 & s_{16} \\ s_{12} & s_{22} & 0 & 0 & s_{26} \\ 0 & 0 & s_{44} & s_{45} & 0 \\ 0 & 0 & s_{45} & s_{55} & 0 \\ s_{16} & s_{26} & 0 & 0 & s_{66} \end{bmatrix} \begin{Bmatrix} \sigma_1 \\ \sigma_2 \\ \sigma_4 \\ \sigma_5 \\ \sigma_6 \end{Bmatrix} + \begin{bmatrix} 0 & 0 & d_{31} \\ 0 & 0 & d_{32} \\ d_{14} & d_{24} & 0 \\ d_{15} & d_{25} & 0 \\ 0 & 0 & d_{36} \end{bmatrix} \begin{Bmatrix} E_1 \\ E_2 \\ E_3 \end{Bmatrix} + \begin{Bmatrix} \alpha_1 \\ \alpha_2 \\ 0 \\ 0 \\ 0 \end{Bmatrix} \theta \tag{A-1}$$

$$\begin{Bmatrix} D_1 \\ D_2 \\ D_3 \end{Bmatrix} = \begin{bmatrix} 0 & 0 & d_{14} & d_{15} & 0 \\ 0 & 0 & d_{24} & d_{25} & 0 \\ d_{31} & d_{32} & 0 & 0 & d_{36} \end{bmatrix} \begin{Bmatrix} \sigma_1 \\ \sigma_2 \\ \sigma_4 \\ \sigma_5 \\ \sigma_6 \end{Bmatrix} + \begin{bmatrix} \epsilon_{11} & 0 & 0 \\ 0 & \epsilon_{22} & 0 \\ 0 & 0 & \epsilon_{33} \end{bmatrix} \begin{Bmatrix} E_1 \\ E_2 \\ E_3 \end{Bmatrix} + \begin{Bmatrix} p_1 \\ p_2 \\ p_3 \end{Bmatrix} \theta \tag{A-2}$$

or in semi-inverted form

$$\begin{Bmatrix} \sigma_1 \\ \sigma_2 \\ \sigma_4 \\ \sigma_5 \\ \sigma_6 \end{Bmatrix} = \begin{bmatrix} C_{11} & C_{12} & 0 & 0 & C_{16} \\ C_{12} & C_{22} & 0 & 0 & C_{26} \\ 0 & 0 & C_{44} & C_{45} & 0 \\ 0 & 0 & C_{45} & C_{55} & 0 \\ C_{16} & C_{26} & 0 & 0 & C_{66} \end{bmatrix} \begin{Bmatrix} S_1 \\ S_2 \\ S_4 \\ S_5 \\ S_6 \end{Bmatrix} - \begin{bmatrix} 0 & 0 & e_{31} \\ 0 & 0 & e_{32} \\ e_{14} & e_{24} & 0 \\ e_{15} & e_{25} & 0 \\ 0 & 0 & e_{36} \end{bmatrix} \begin{Bmatrix} E_1 \\ E_2 \\ E_3 \end{Bmatrix} - \begin{Bmatrix} \lambda_1 \\ \lambda_2 \\ 0 \\ 0 \\ 0 \end{Bmatrix} \theta \tag{A-3}$$

$$\begin{Bmatrix} D_1 \\ D_2 \\ D_3 \end{Bmatrix} = \begin{bmatrix} 0 & 0 & e_{14} & e_{15} & 0 \\ 0 & 0 & e_{24} & e_{25} & 0 \\ e_{31} & e_{32} & 0 & 0 & e_{36} \end{bmatrix} \begin{Bmatrix} S_1 \\ S_2 \\ S_4 \\ S_5 \\ S_6 \end{Bmatrix} + \begin{bmatrix} \epsilon_{11} & 0 & 0 \\ 0 & \epsilon_{22} & 0 \\ 0 & 0 & \epsilon_{33} \end{bmatrix} \begin{Bmatrix} E_1 \\ E_2 \\ E_3 \end{Bmatrix} + \begin{Bmatrix} p_1 \\ p_2 \\ p_3 \end{Bmatrix} \theta \tag{A-4}$$

Appendix B:

Generalized Laminate Matrices for a Constant Through-the-Thickness Displacement Plate

If L is the number of composite plies and piezoelectric layers, the laminate density matrix is

$$P_{ij}^{km} = \sum_{l=1}^{L} \int_{z} \rho \ \psi^{k}(z) \ \psi^{m}(z) \ dz \tag{B-1}$$

for ij = 11 and 22, while

$$P_{33} = \sum_{l=1}^{L} \int_{z} \rho \ dz \tag{B-2}$$

The laminate stiffness matrices are

$$A_{ij}^{km} = \sum_{l=1}^{L} \int_{z} C_{ij} \ \psi^{k}(z) \ \psi^{m}(z) \ dz \tag{B-3}$$

for ij = 11, 12, 16, 22, 26, 44, and 66;

$$B_{ij}^{k} = \sum_{l=1}^{L} \int_{z} C_{ij} \ \frac{\partial \psi^{k}(z)}{\partial z} \ dz \tag{B-4}$$

$$\overline{C_{ij}} = \sum_{l=1}^{L} \int_{z} C_{ij} \ dz \tag{B-5}$$

$$D_{ij}^{km} = \sum_{l=1}^{L} \int_{z} C_{ij} \ \frac{\partial \psi^{k}(z)}{\partial z} \ \frac{\partial \psi^{m}(z)}{\partial z} \ dz \tag{B-6}$$

for ij = 44, 45, and 55. The laminate piezoelectric matrices are

$$E_{ij}^{km} = \sum_{l=1}^{L} \int_{z} e_{ij} \ \psi^{k}(z) \ \frac{\partial \psi^{m}(z)}{\partial z} \ dz \tag{B-7}$$

$$\overline{E_{ij}^{km}} = \sum_{l=1}^{L} \int_{z} e_{ij} \ \frac{\partial \psi^{k}(z)}{\partial z} \ \psi^{m}(z) \ dz \tag{B-8}$$

for ij = 31, 32, and 36. The laminate dielectric permittivity matrix is

$$G_{ij}^{km} = \sum_{l=1}^{L} \int_{z} \epsilon_{ij} \, \psi^{k}(z) \, \psi^{m}(z) \, dz \qquad \text{(B-9)}$$

for ij = 11 and 22, while

$$G_{33}^{km} = \sum_{l=1}^{L} \int_{z} \epsilon_{33} \, \frac{\partial \psi^{k}(z)}{\partial z} \, \frac{\partial \psi^{m}(z)}{\partial z} \, dz \qquad \text{(B-10)}$$

The laminate thermal force vector is

$$f_{i,th}^{k} = \sum_{l=1}^{L} \int_{z} \lambda_{i} \, \psi_{j} \, \theta_{j} \, \psi^{k}(z) \, dz \qquad \text{(B-11)}$$

for i = 1 and 2. The laminate thermal electric displacement vector is

$$q_{i,th}^{k} = \sum_{l=1}^{L} \int_{z} p_{i} \, \psi_{j} \, \theta_{j} \, \psi^{k}(z) \, dz \qquad \text{(B-12)}$$

for i =1 and 2, while

$$q_{3,th}^{k} = \sum_{l=1}^{L} \int_{z} p_{3} \, \psi_{j} \, \theta_{j} \, \frac{\partial \psi^{k}(z)}{\partial z} \, dz \qquad \text{(B-13)}$$

Appendix C:

Finite Element Submatrices for a Constant Through-the-Thickness Displacement Plate

The mass submatrices are

$$[M_{ij}]^{pq} = \int_A [P_{ij}]\, R^p(x,y)\, R^q(x,y)\, dA \tag{C-1}$$

The stiffness submatrices are

$$[K_{11}]^{pq} = \int_A \{\, [A_{11}] \frac{\partial R^p}{\partial x} \frac{\partial R^q}{\partial x} + [A_{16}] \left(\frac{\partial R^p}{\partial x} \frac{\partial R^q}{\partial y} + \frac{\partial R^p}{\partial y} \frac{\partial R^q}{\partial x}\right) + [D_{55}]\, R^p\, R^q + [A_{66}] \frac{\partial R^p}{\partial y} \frac{\partial R^q}{\partial y} \,\}\, dA \tag{C-2}$$

$$[K_{12}]^{pq} = \int_A \{\, [A_{12}] \frac{\partial R^p}{\partial x} \frac{\partial R^q}{\partial y} + [A_{16}] \frac{\partial R^p}{\partial x} \frac{\partial R^q}{\partial x} + [A_{26}] \frac{\partial R^p}{\partial y} \frac{\partial R^q}{\partial y} + [D_{45}]\, R^p\, R^q + [A_{66}] \frac{\partial R^p}{\partial y} \frac{\partial R^q}{\partial x} \,\}\, dA \tag{C-3}$$

$$[K_{13}]^{pq} = \int_A \{\, [B_{45}]\, R^p \frac{\partial R^q}{\partial y} + [B_{55}]\, R^p \frac{\partial R^q}{\partial x} \,\}\, dA \tag{C-4}$$

$$[K_{14}]^{pq} = \int_A \{\, [E_{31}] \frac{\partial R^p}{\partial x} R^q + [E_{36}] \frac{\partial R^p}{\partial y} R^q \,\}\, dA \tag{C-5}$$

$$[K_{22}]^{pq} = \int_A \{\, [A_{22}] \frac{\partial R^p}{\partial y} \frac{\partial R^q}{\partial y} + [A_{26}] \left(\frac{\partial R^p}{\partial x} \frac{\partial R^q}{\partial y} + \frac{\partial R^p}{\partial y} \frac{\partial R^q}{\partial x}\right) + [D_{44}]\, R^p\, R^q + [A_{66}] \frac{\partial R^p}{\partial x} \frac{\partial R^q}{\partial x} \,\}\, dA \tag{C-6}$$

$$[K_{23}]^{pq} = \int_A \{ [B_{44}] R^p \frac{\partial R^q}{\partial y} + [B_{45}] R^p \frac{\partial R^q}{\partial x} \} dA \quad \text{(C-7)}$$

$$[K_{24}]^{pq} = \int_A \{ [E_{32}] \frac{\partial R^p}{\partial y} R^q + [E_{36}] \frac{\partial R^p}{\partial x} R^q \} dA \quad \text{(C-8)}$$

$$[K_{33}]^{pq} = \int_A \{ [\overline{C_{44}}] \frac{\partial R^p}{\partial y} \frac{\partial R^q}{\partial y} + [\overline{C_{45}}] (\frac{\partial R^p}{\partial x} \frac{\partial R^q}{\partial y} + \frac{\partial R^p}{\partial y} \frac{\partial R^q}{\partial x}) + [\overline{C_{55}}] \frac{\partial R^p}{\partial x} \frac{\partial R^q}{\partial x} \} dA \quad \text{(C-9)}$$

$$[K_{44}]^{pq} = \int_A \{ [G_{11}] \frac{\partial R^p}{\partial x} \frac{\partial R^q}{\partial x} + [G_{22}] \frac{\partial R^p}{\partial y} \frac{\partial R^q}{\partial y} + [G_{33}] R^p R^q \} dA \quad \text{(C-10)}$$

The external forces are

$$[F_i]^p = \int_A t_i R^p(x,y) dA \quad \text{(C-11)}$$

$$[Q]^p = \int_{A_p} q R^p(x,y) dA \quad \text{(C-12)}$$

The thermal forces are

$$[F_{1,th}]^p = \int_A f_{1,th} \frac{\partial R^p(x,y)}{\partial x} dA \quad \text{(C-13)}$$

$$[F_{2,th}]^p = \int_A f_{2,th} \frac{\partial R^p(x,y)}{\partial y} dA \quad \text{(C-14)}$$

$$[Q_{th}]^p = \int_{A_p} \{ q_{1,th} \frac{\partial R^p}{\partial x} + q_{2,th} \frac{\partial R^p}{\partial y} + q_{3,th} R^p \} dA \quad \text{(C-15)}$$

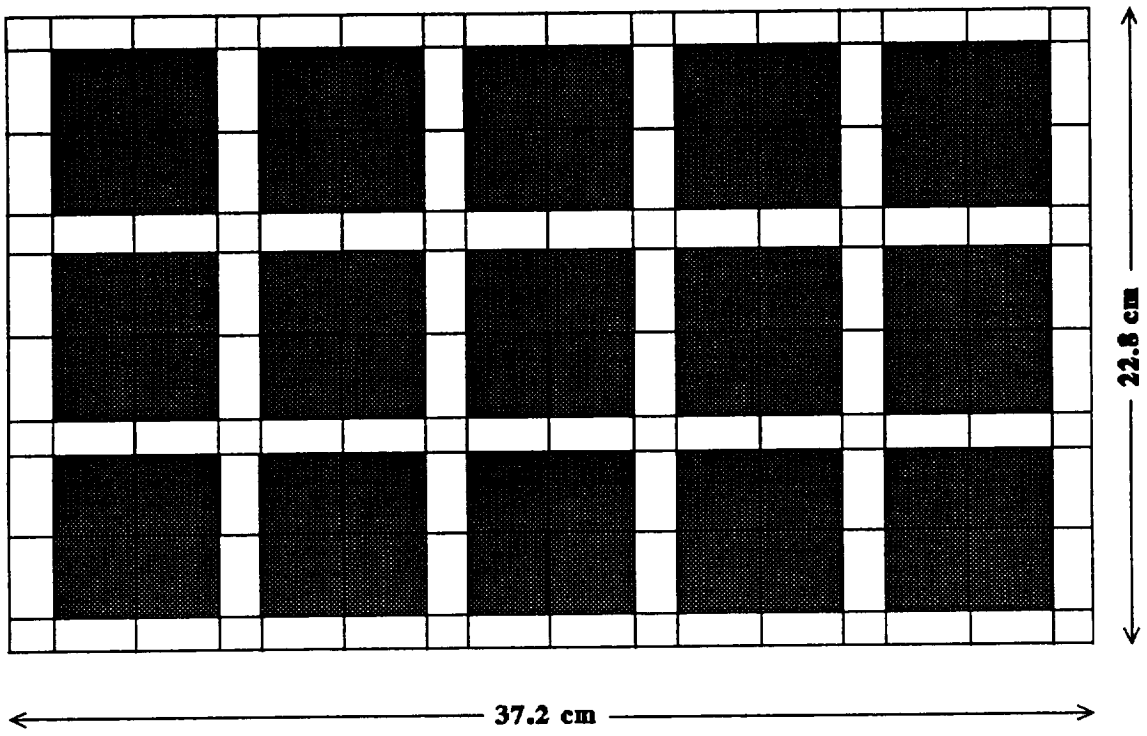

Figure 1: Model of Graphite/Epoxy Plate with Attached Piezoceramic Patches
(a) Top View

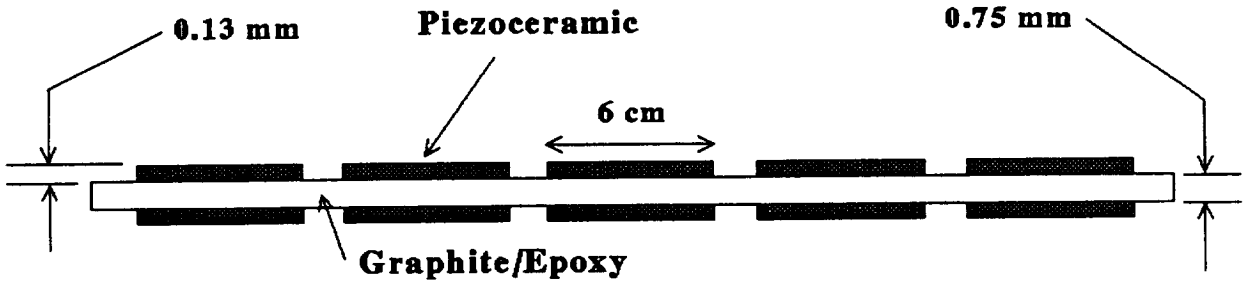

Figure 1: Model of Graphite/Epoxy Plate with Attached Piezoceramic Patches
(b) Front View

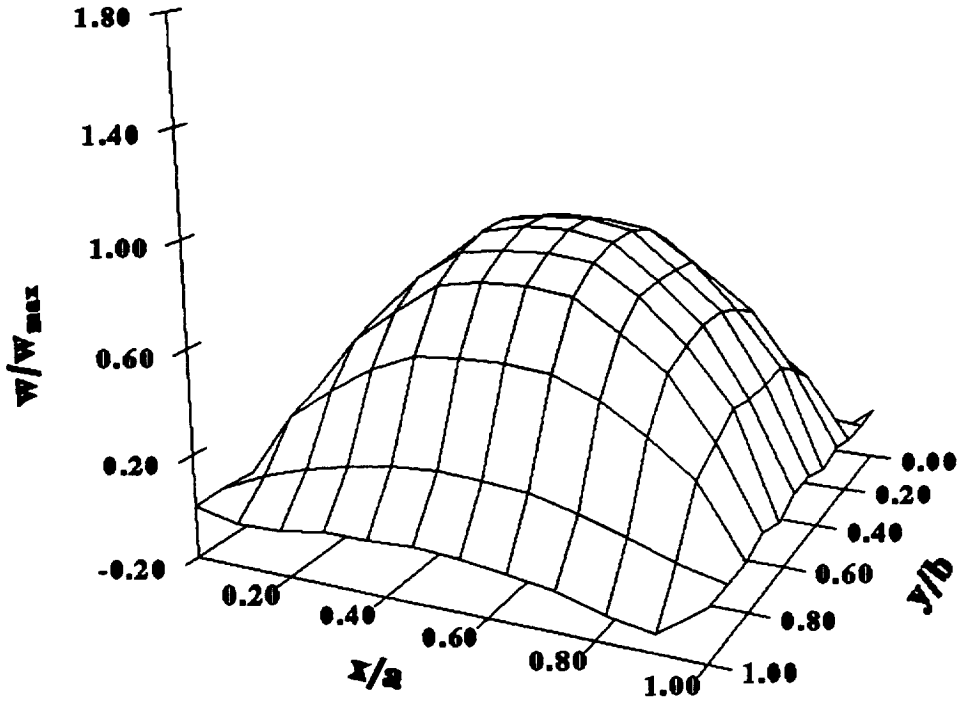

Figure 2: Active Compensation of Thermal Deformation of $[0/\pm45]_s$ Plate Subject to 100°C Gradient (a): 0 Volts Applied on Upper and Lower Piezoceramic Patches

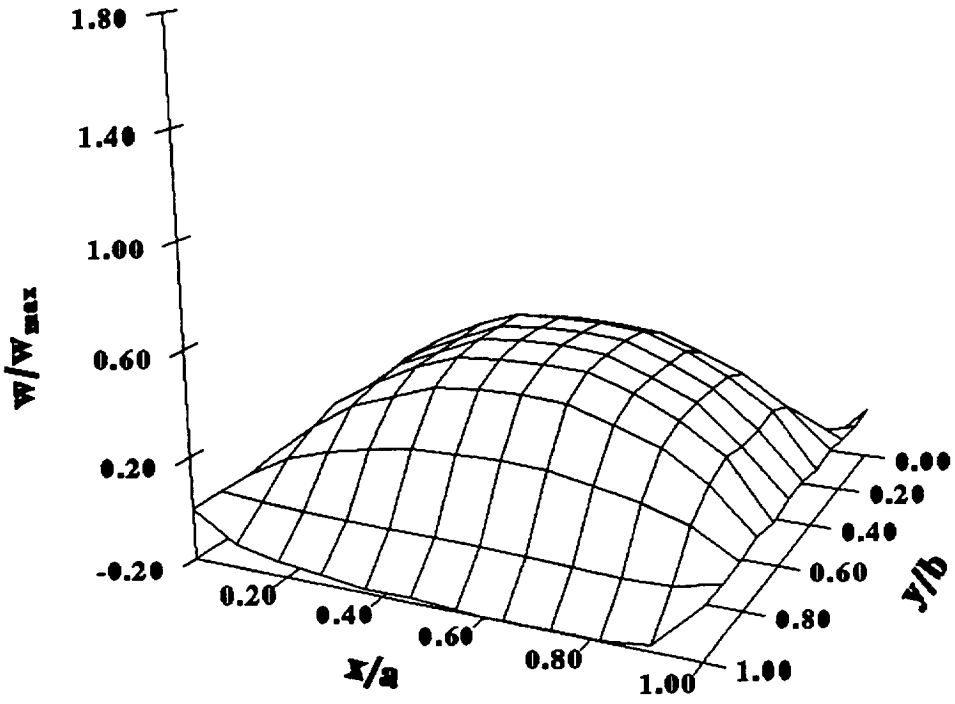

Figure 2: Compensation of Thermal Deformation of $[0/\pm45]_s$ Plate Subject to 100°C Gradient (b): 34 Volts Applied on Upper and Lower Piezoceramic Patches

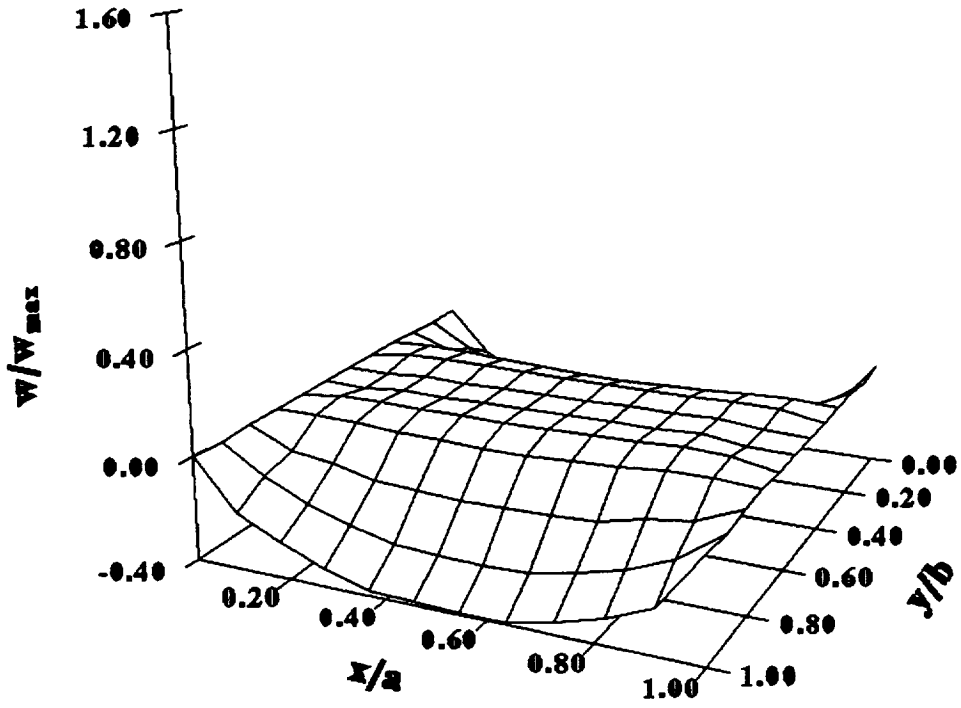

Figure 2: Compensation of Thermal Deformation of $[0/\pm45]_s$ Plate Subject to 100°C Gradient (c): 70 Volts Applied on Upper and Lower Piezoceramic Patches

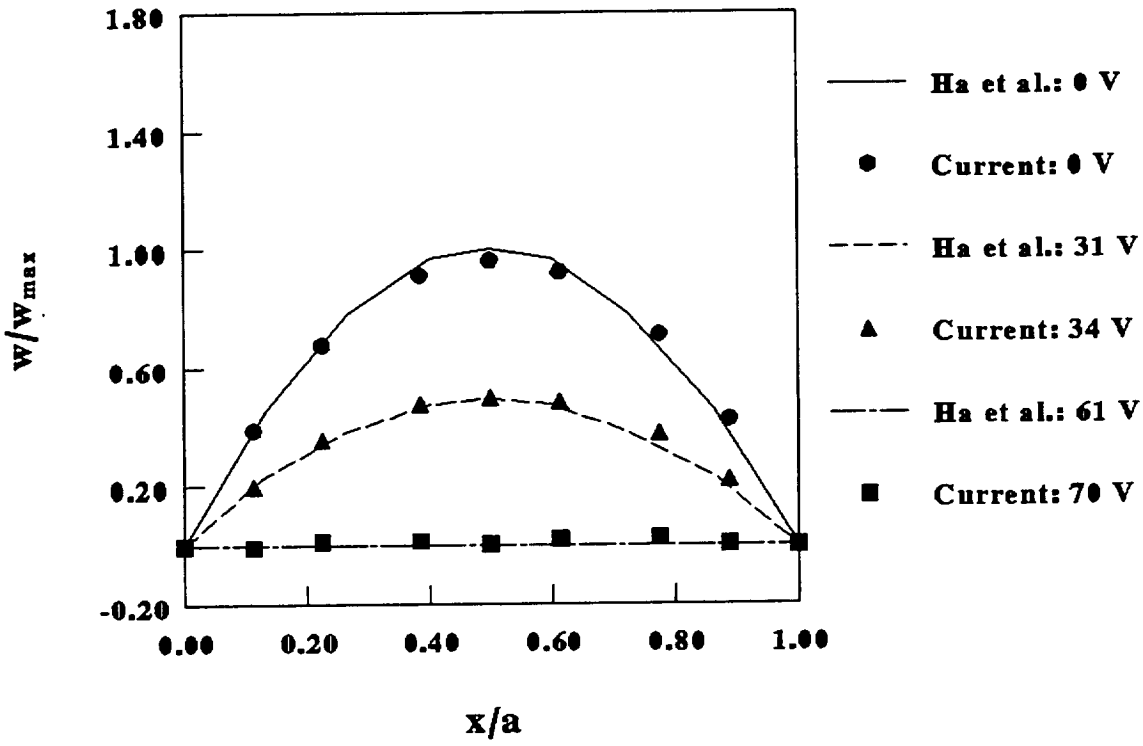

Figure 3: Centerline (y/b=0.5) Deflections of $[0/\pm45]_s$ Plate

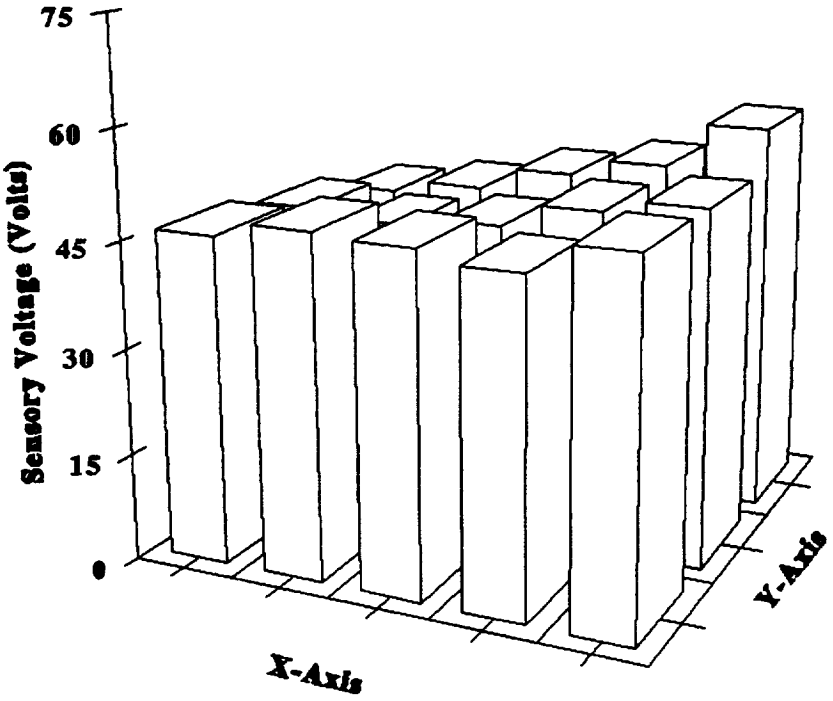

Figure 4: Sensory Voltages on Upper Piezoceramic Patches of a $[0/\pm45]_s$ Plate Subject to 100°C Gradient (a): 0 Volts Applied on Lower Piezoceramic Patches

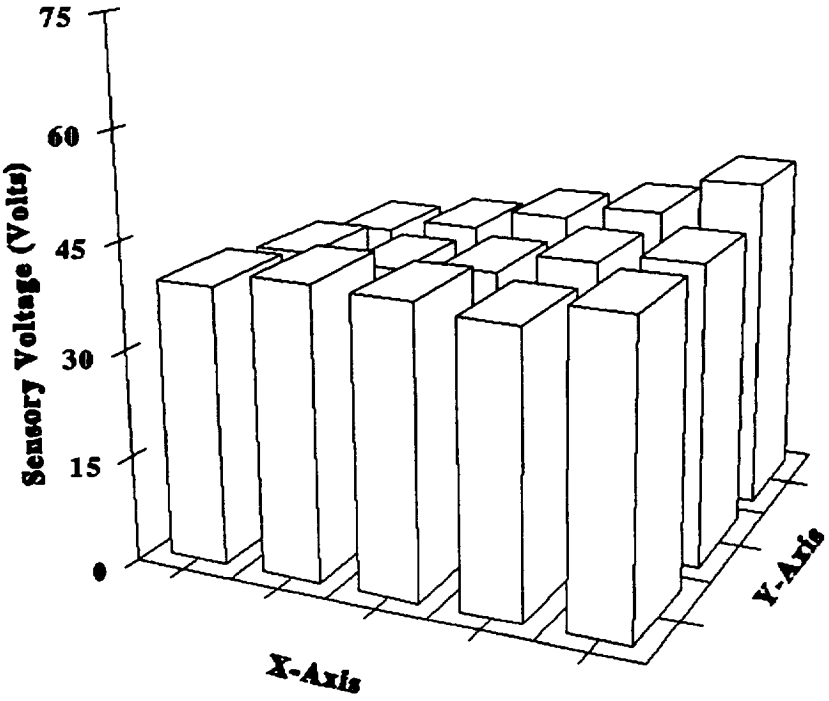

Figure 4: Sensory Voltages on Upper Piezoceramic Patches of a $[0/\pm45]_s$ Plate Subject to 100°C Gradient (b): 34 Volts Applied on Lower Piezoceramic Patches

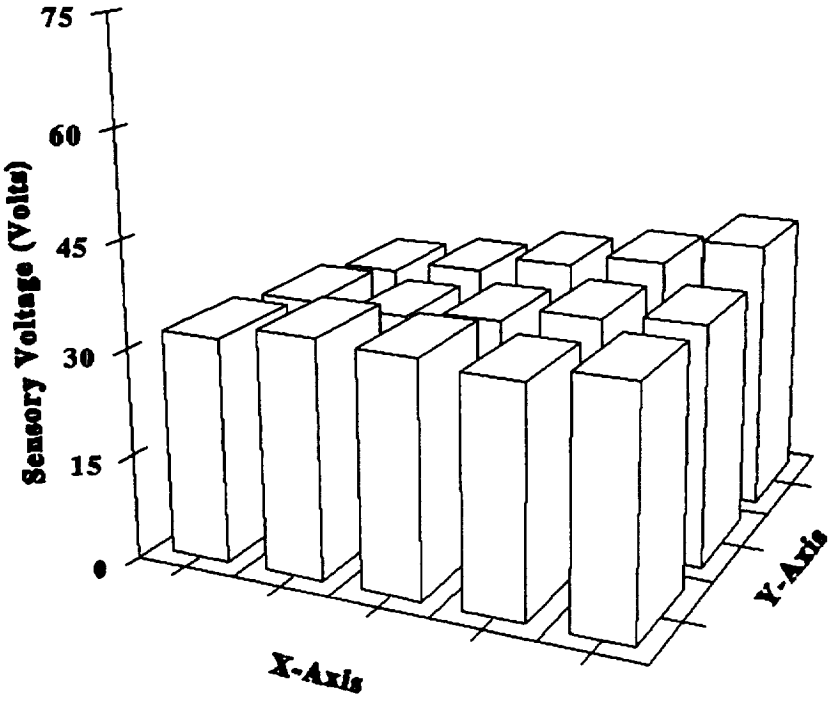

Figure 4: Sensory Voltages on Upper Piezoceramic Patches of a $[0/\pm45]_s$ Plate Subject to 100°C Gradient (c): 70 Volts Applied on Lower Piezoceramic Patches

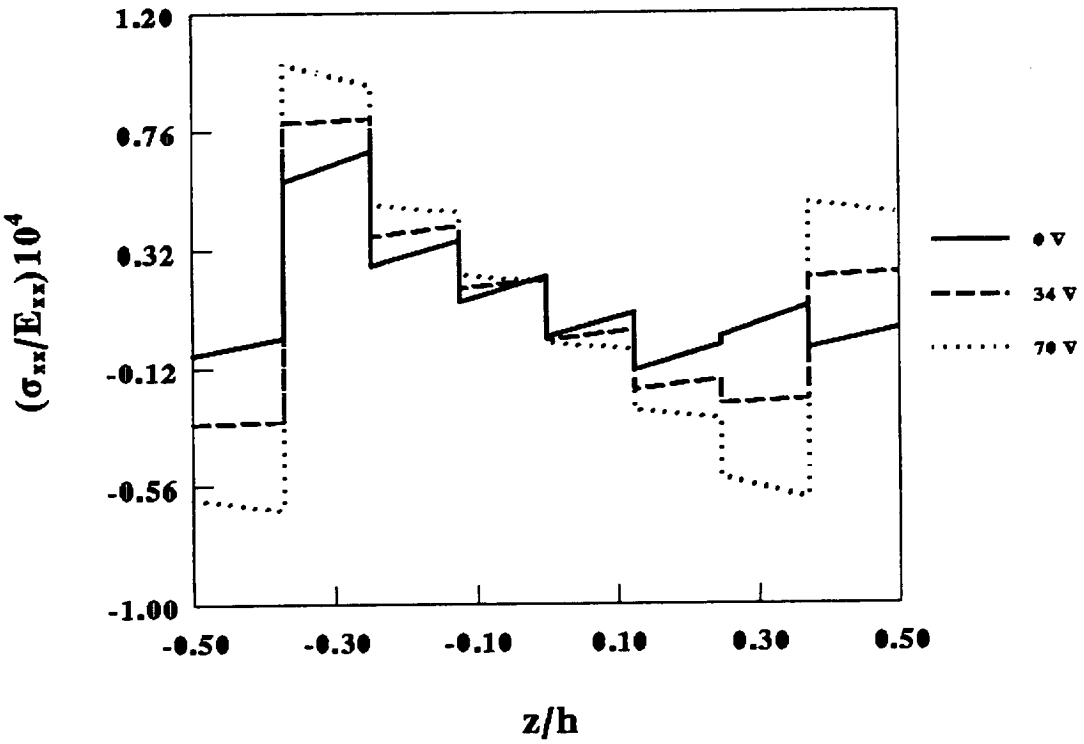

Figure 5: Through-The-Thickness Stresses in $[0/\pm45]_s$ Plate Subject to 100°C Gradient with Different Applied Voltages on Upper and Lower Piezoceramic Patches (a): σ_{xx}

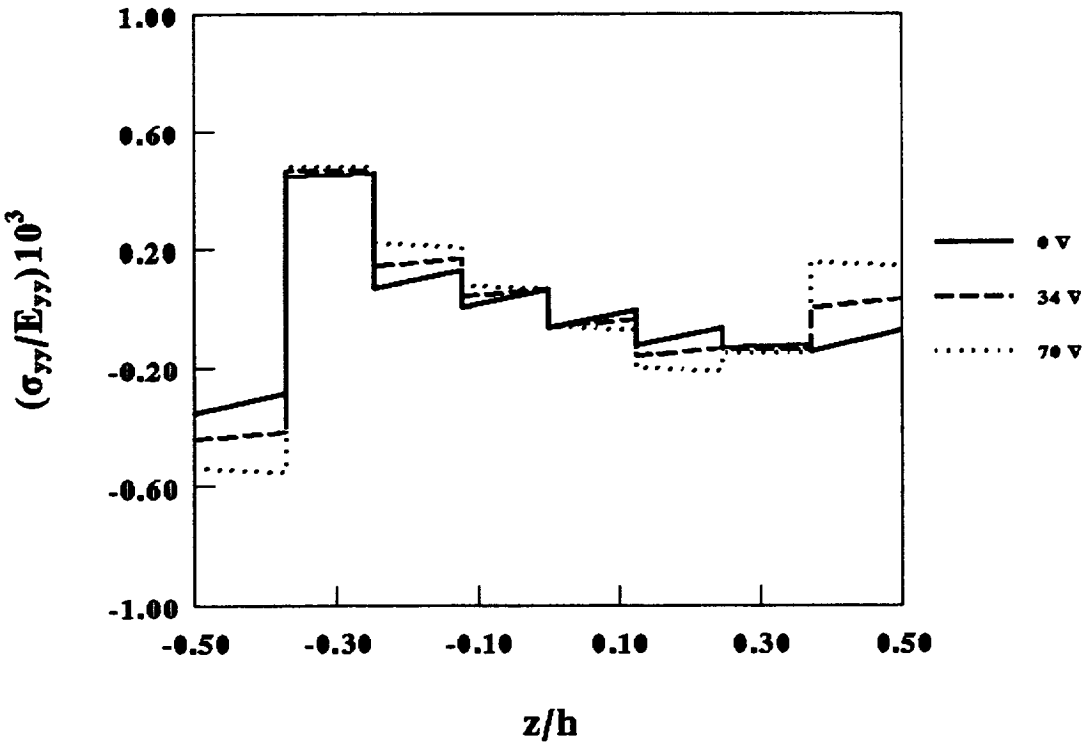

Figure 5: Through-The-Thickness Stresses in [0/±45]$_s$ Plate Subject to 100°C Gradient with Different Applied Voltages on Upper and Lower Piezoceramic Patches (b): σ_{yy}

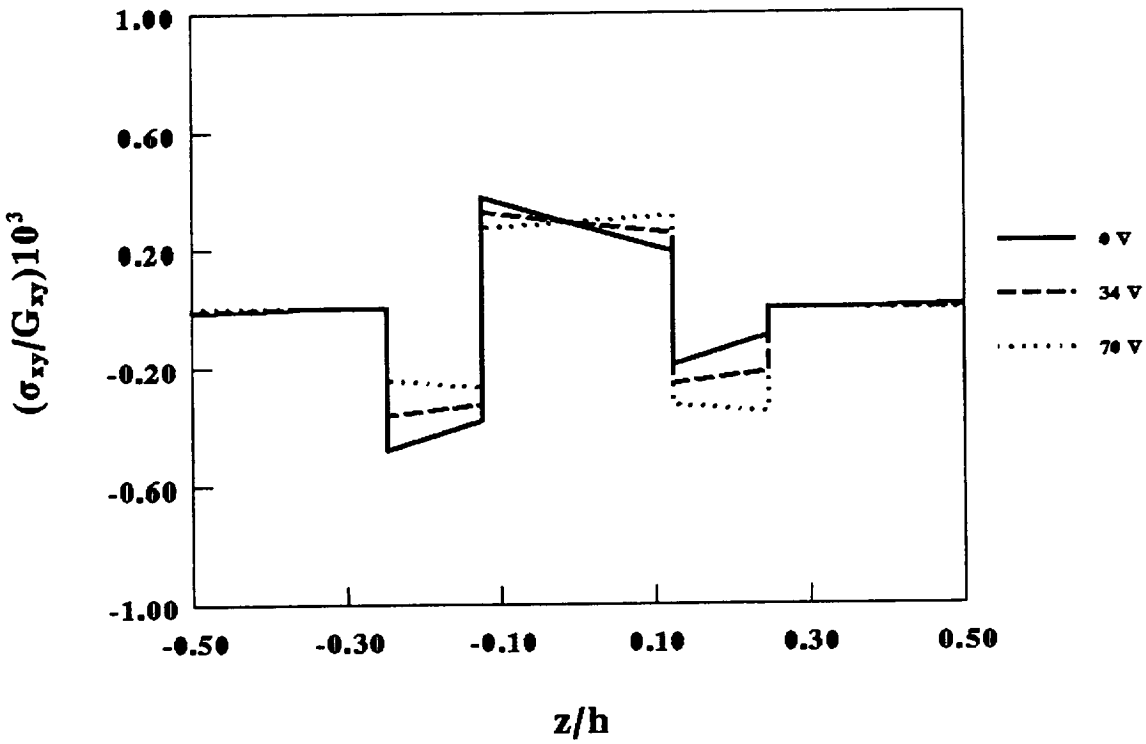

Figure 5: Through-The-Thickness Stresses in $[0/\pm45]_s$ Plate Subject to 100°C Gradient with Different Applied Voltages on Upper and Lower Piezoceramic Patches (c): σ_{xy}

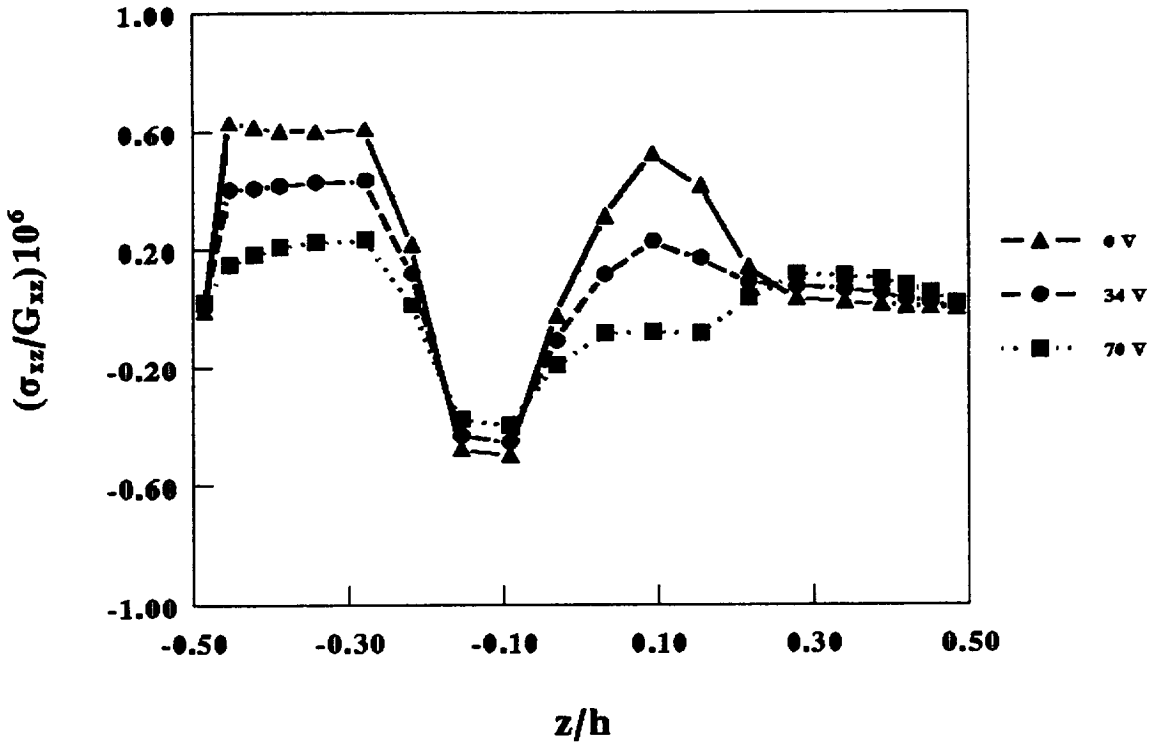

Figure 5: Through-The-Thickness Stresses in $[0/\pm45]_s$ Plate Subject to 100°C Gradient with Different Applied Voltages on Upper and Lower Piezoceramic Patches (d): σ_{xz}

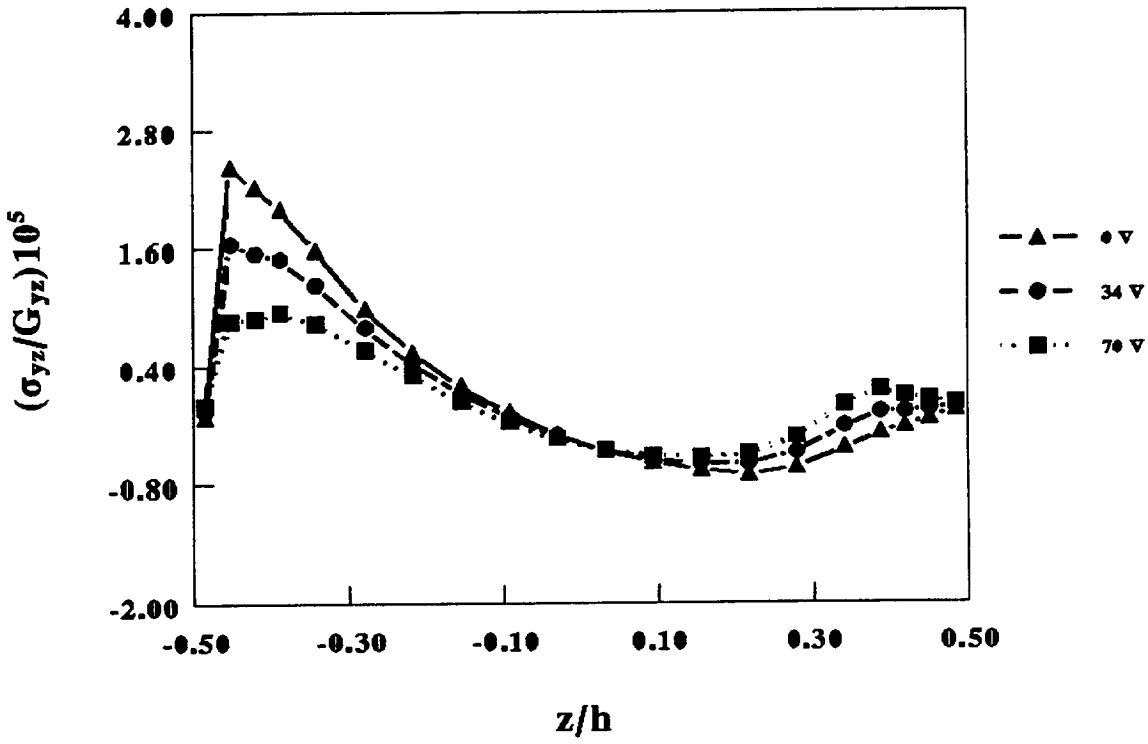

Figure 5: Through-The-Thickness Stresses in $[0/\pm45]_s$ Plate Subject to 100°C Gradient with Different Applied Voltages on Upper and Lower Piezoceramic Patches (e): σ_{yz}

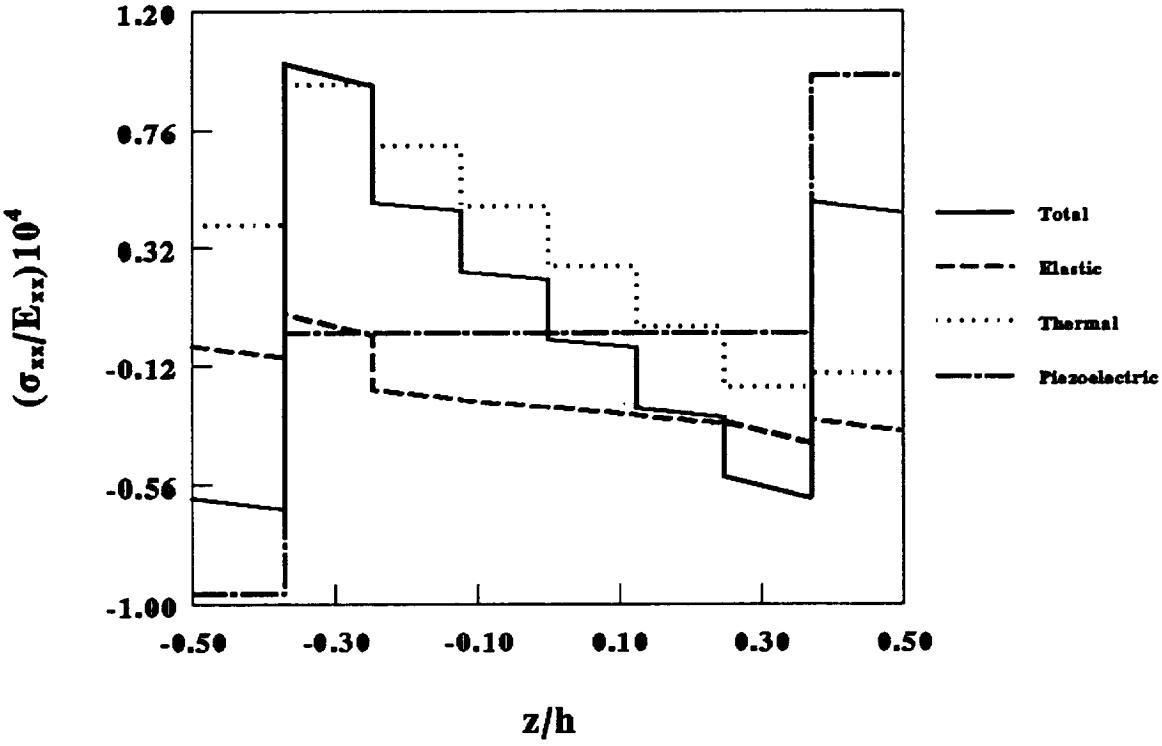

Figure 6: Elastic, Thermal, and Piezoelectric Stress Components in $[0/\pm45]_s$ Plate Subject to 100°C Gradient with 70 Volts Applied on Upper and Lower Surface Piezoceramic Patches (a): σ_{xx}

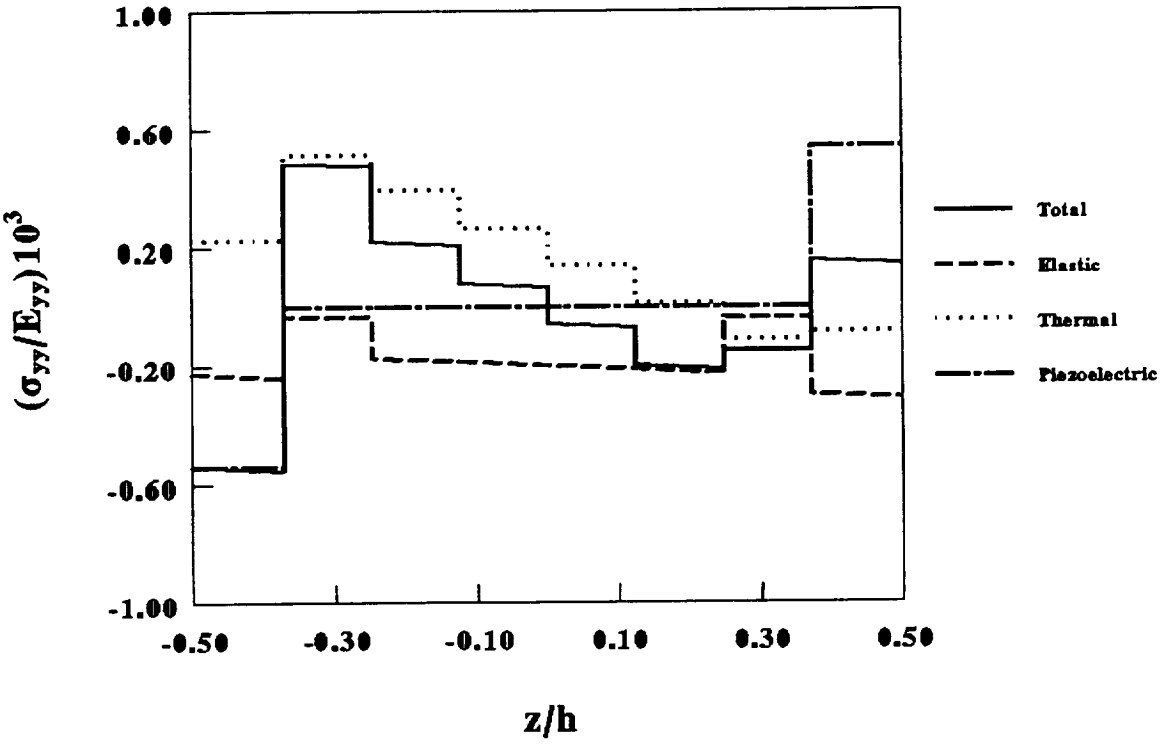

Figure 6: Elastic, Thermal, and Piezoelectric Stress Components in $[0/\pm45]_s$ Plate Subject to 100°C Gradient with 70 Volts Applied on Upper and Lower Surface Piezoceramic Patches (b): σ_{yy}

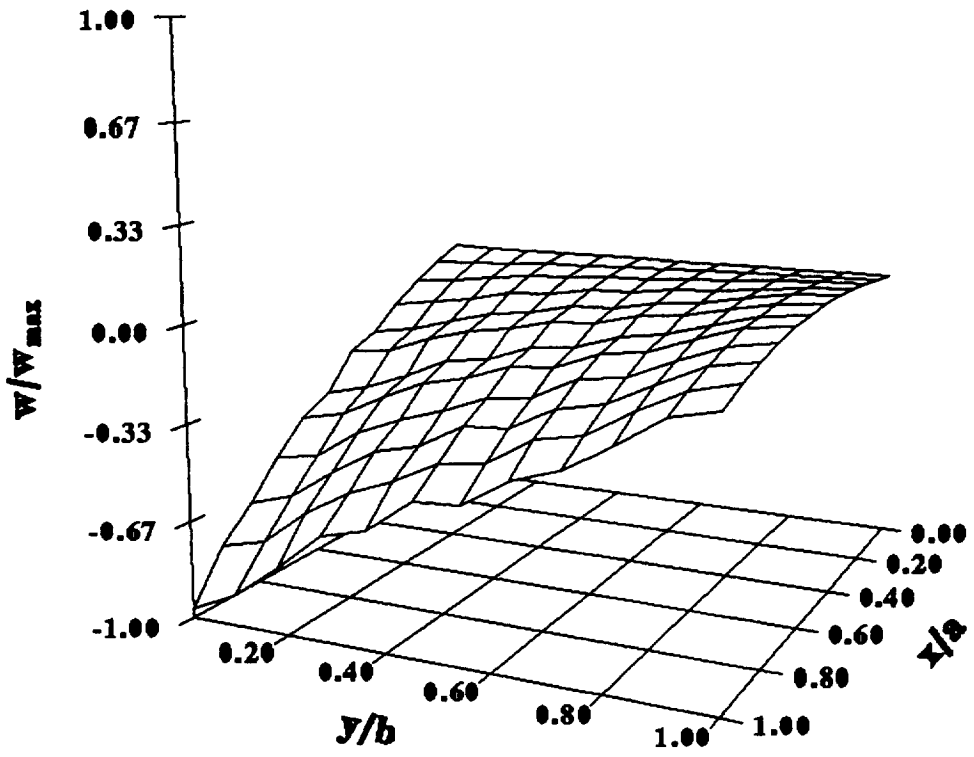

Figure 7: Active Compensation of Thermal Bending and Twisting Deformation of $[45_3/-45_3]$ Plate Subject to 30°C Gradient (a): Initial Thermal Deformation: 0 Volts Applied on Upper and Lower Piezoceramic Actuators

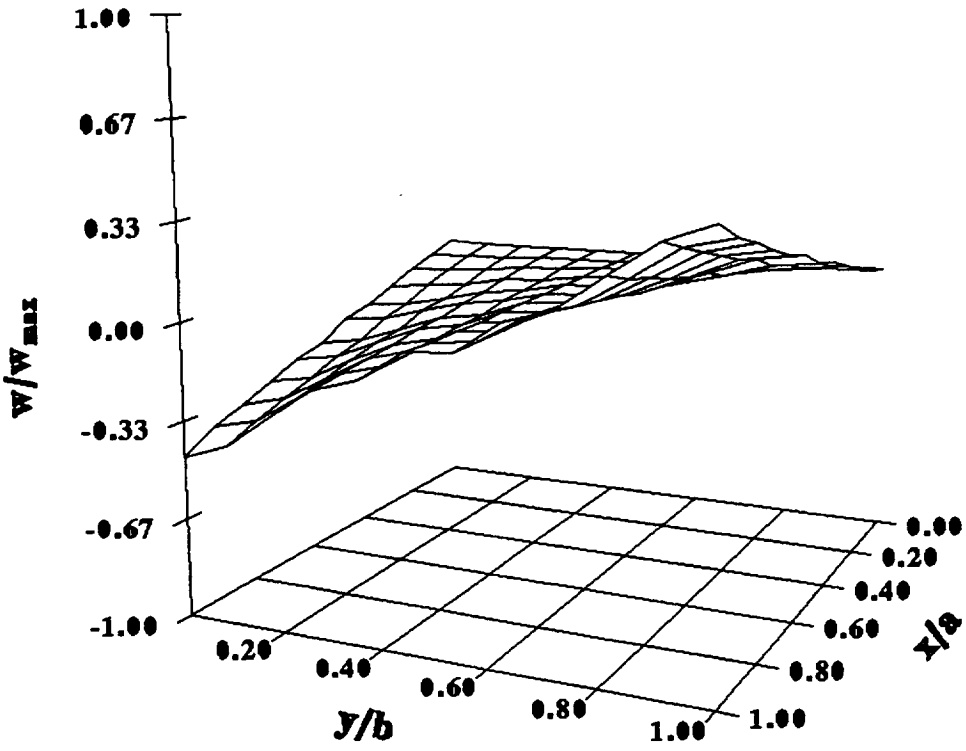

Figure 7: Active Compensation of Thermal Bending and Twisting Deformation of $[45_3/-45_3]$ Plate Subject to 30°C Gradient (b): Active Compensation of Thermal Bending: 40 Volts Applied on Upper and Lower Piezoceramic Actuators

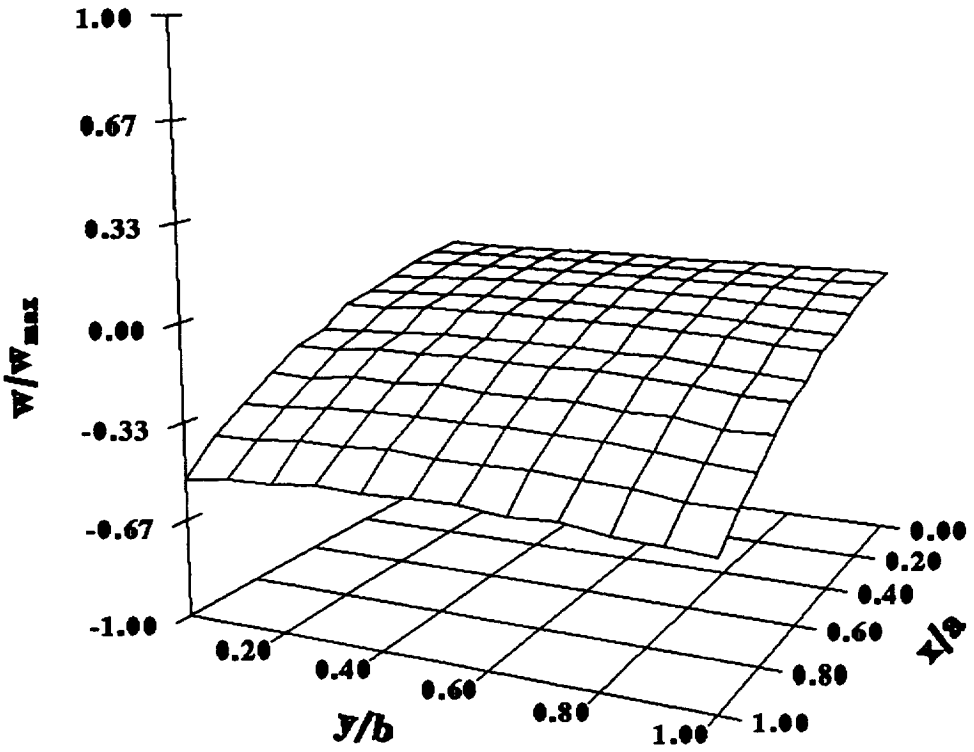

Figure 7: Active Compensation of Thermal Bending and Twisting Deformation of $[45_3/-45_3]$ Plate Subject to 30°C Gradient (c): Active Compensation of Thermal Twisting: 145 Volts Applied on Upper and -145 Volts on Lower Piezoceramic Actuators

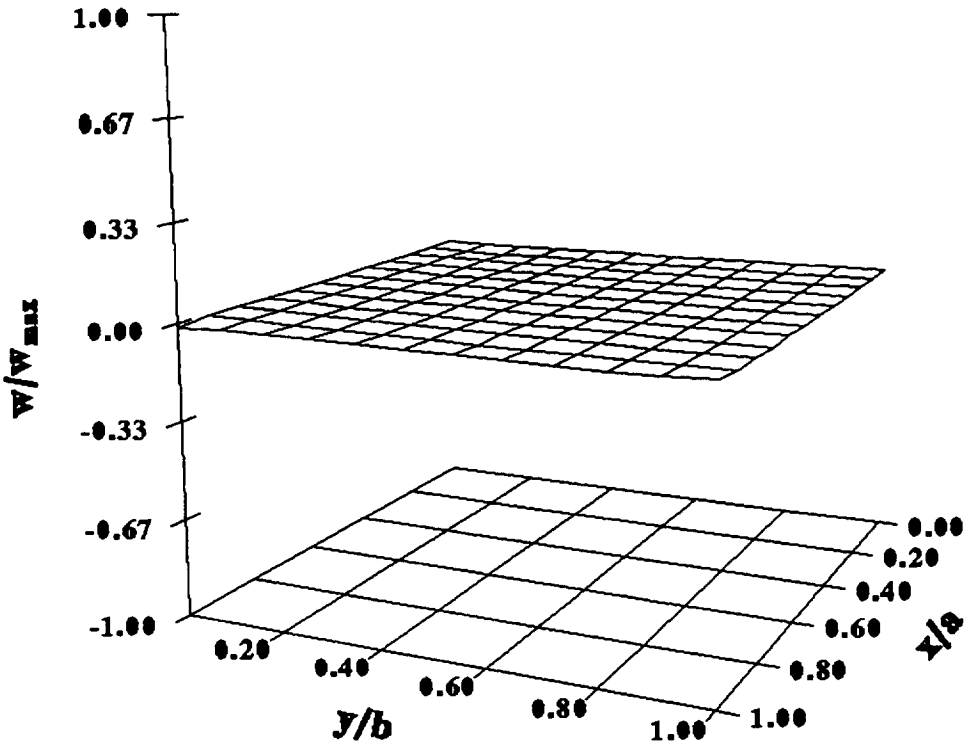

Figure 7: Active Compensation of Thermal Bending and Twisting Deformation of $[45_3/-45_3]$ Plate Subject to 30°C Gradient (d): Complete Compensation of Thermal Deformation: 185 Volts Applied on Upper and -105 Volts on Lower Piezoceramic Actuators

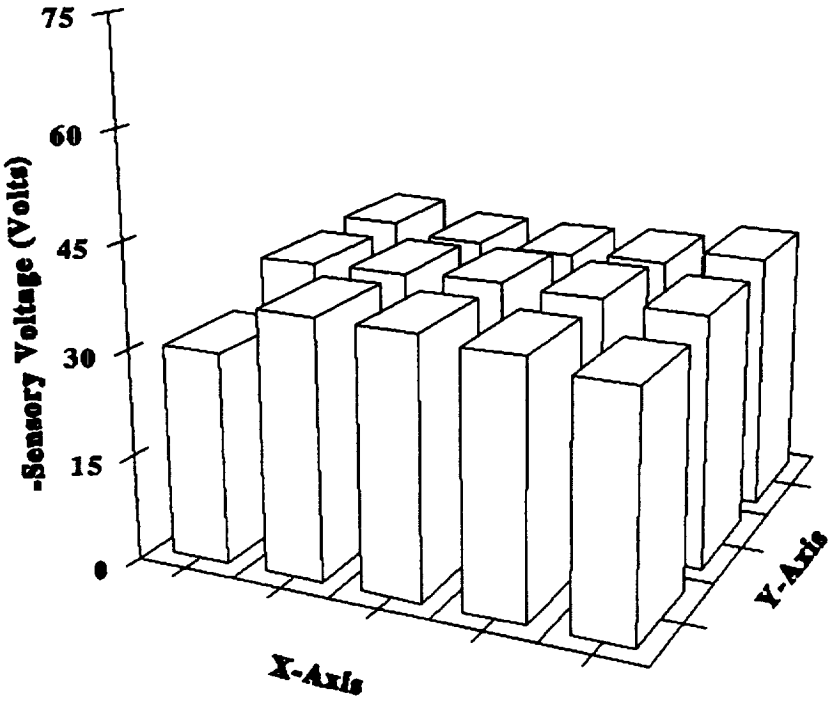

Figure 8: Sensory Voltages on Upper Piezoceramic Patches of a $[45_3/-45_3]$ Plate with 0 Volts Applied on Lower Piezoceramic Patches

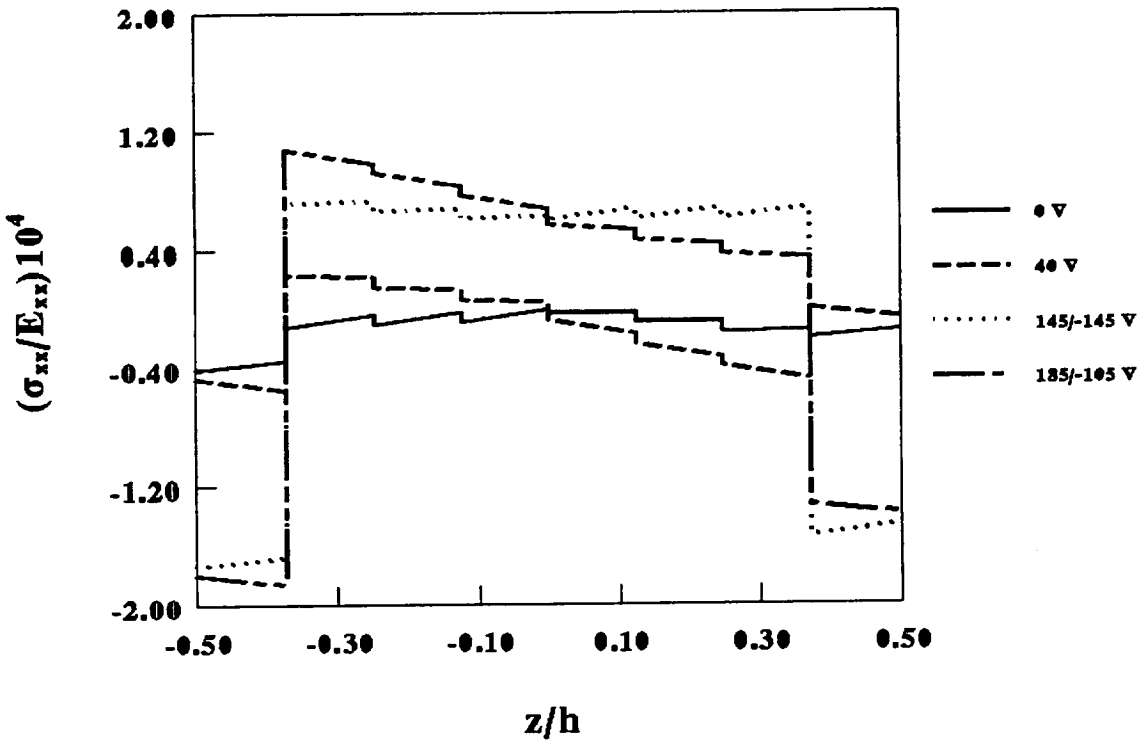

Figure 9: Through-the-Thickness Stress in $[45_3/-45_3]$ Plate Subject to 30°C Gradient with Different Applied Voltages on Upper and Lower Piezoceramic Patches (a): σ_{xx}

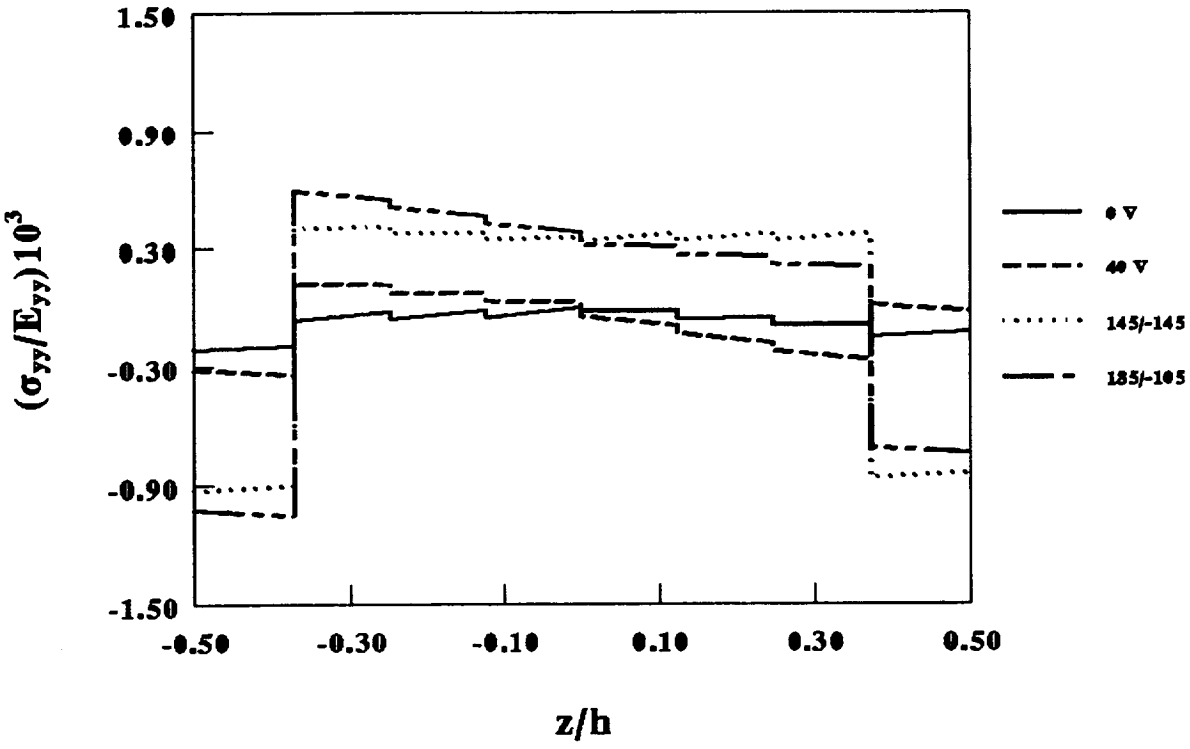

Figure 9: Through-the-Thickness Stress in $[45_3/-45_3]$ Plate Subject to 30°C Gradient with Different Applied Voltages on Upper and Lower Piezoceramic Patches (b): σ_{yy}

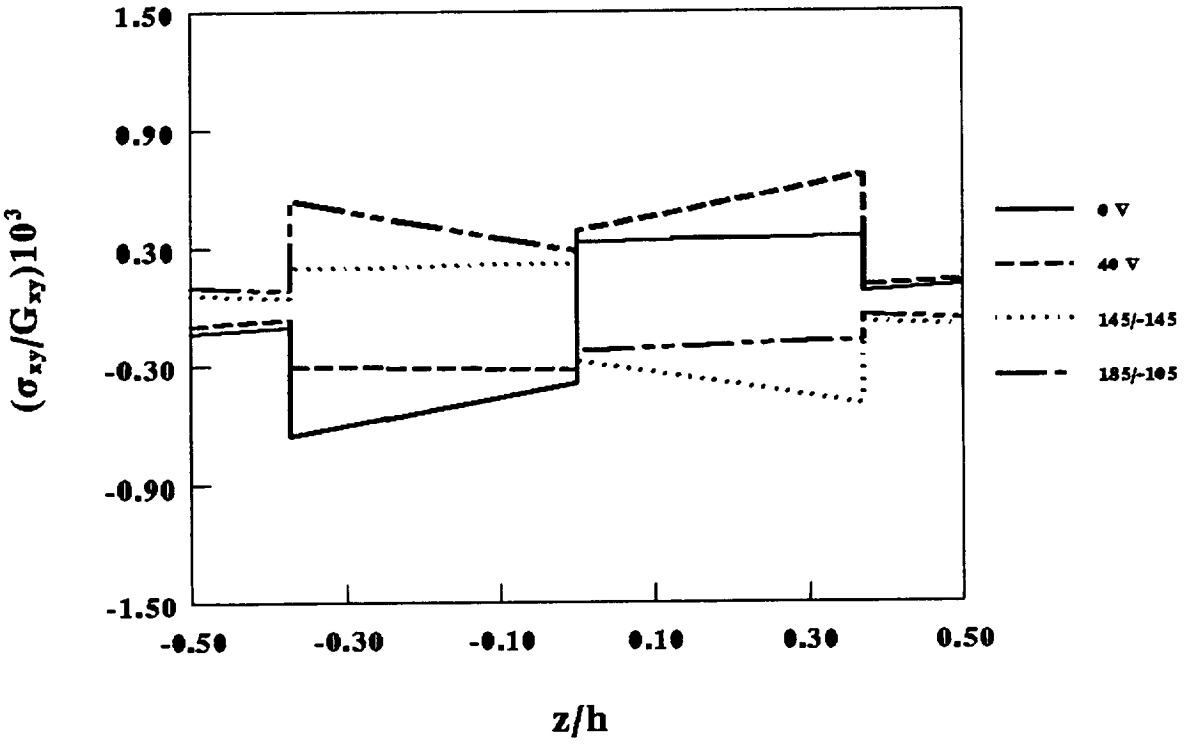

Figure 9: Through-the-Thickness Stress in $[45_3/-45_3]$ Plate Subject to 30°C Gradient with Different Applied Voltages on Upper and Lower Piezoceramic Patches (c): σ_{xy}

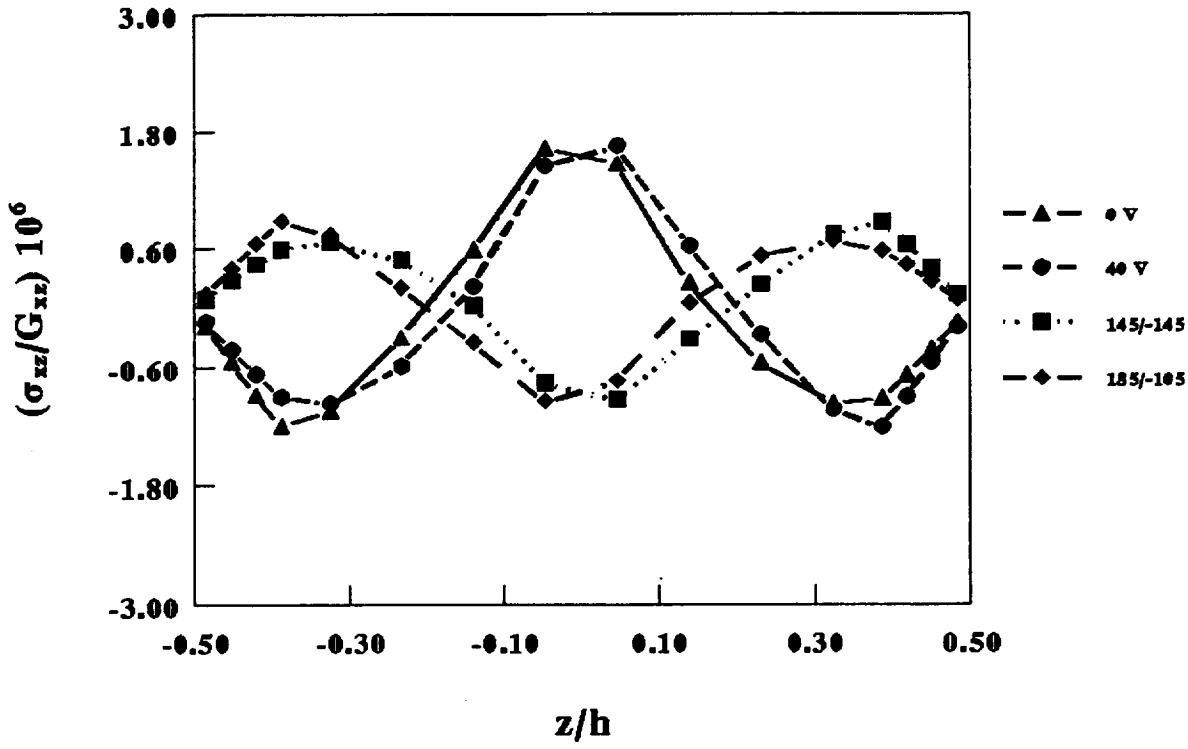

Figure 9: Through-the-Thickness Stress in $[45_3/-45_3]$ Plate Subject to 30°C Gradient with Different Applied Voltages on Upper and Lower Piezoceramic Patches (d): σ_{xz}

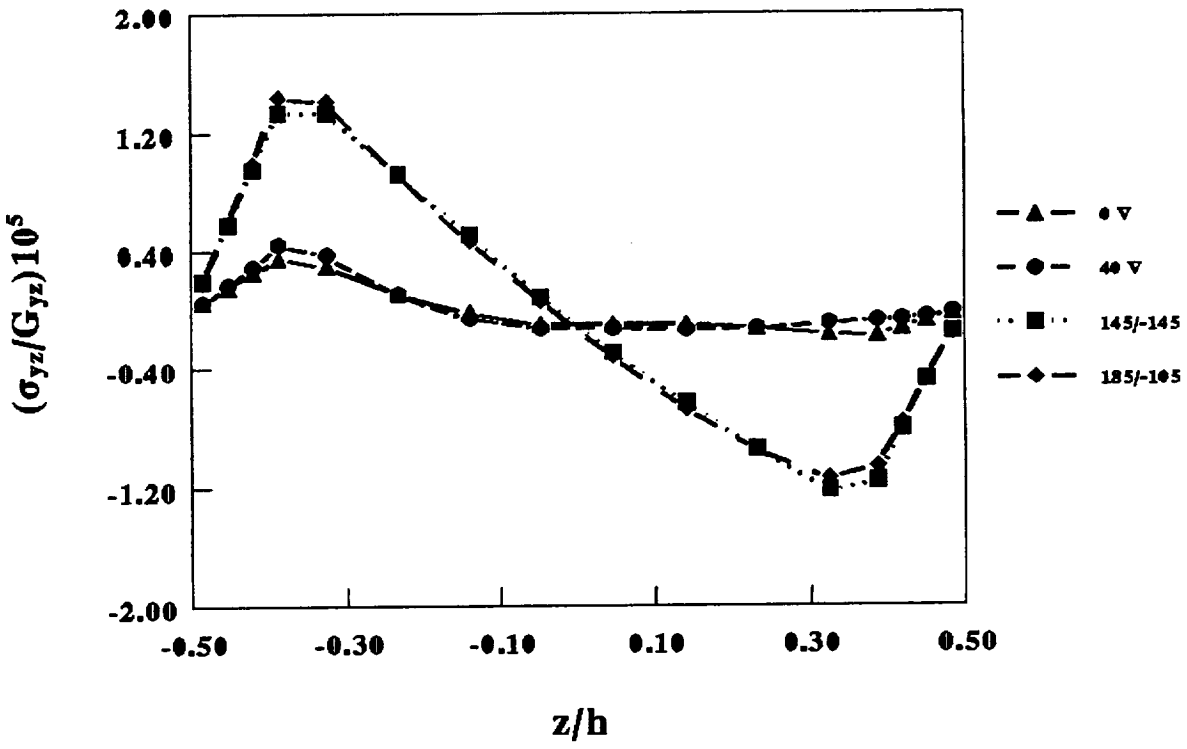

Figure 9: Through-the-Thickness Stress in $[45_3/-45_3]$ Plate Subject to 30°C Gradient with Different Applied Voltages on Upper and Lower Piezoceramic Patches (e): σ_{yz}

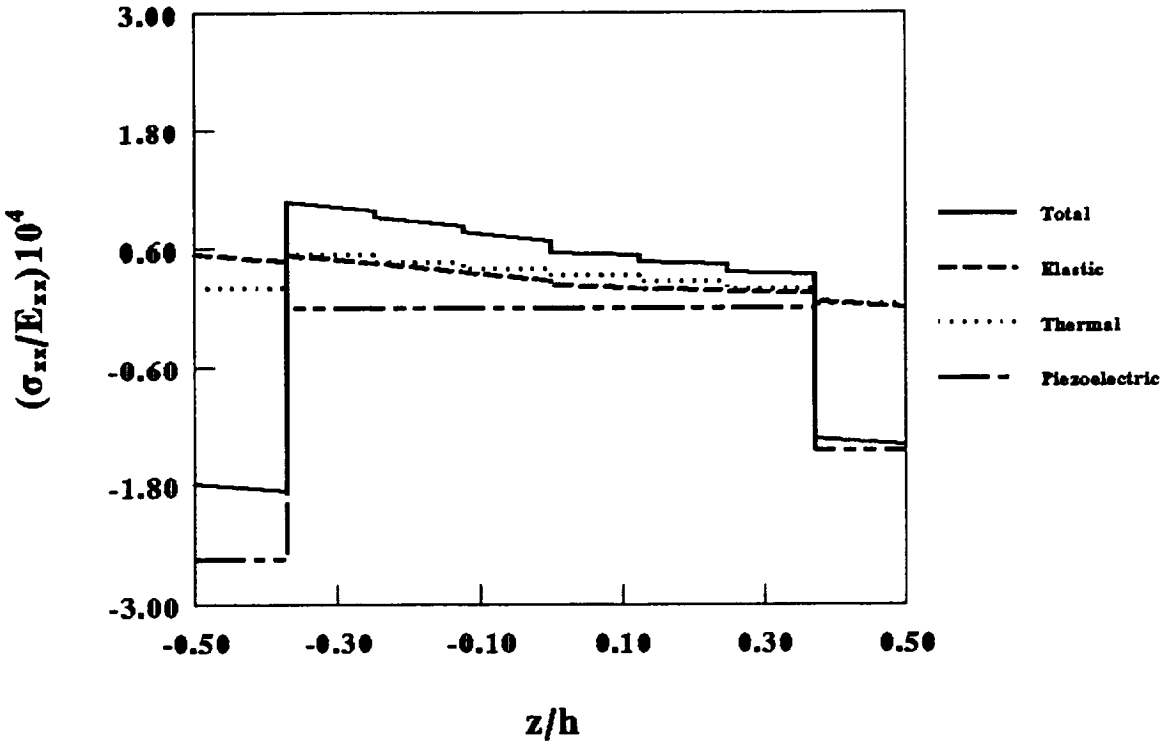

Figure 10: Elastic, Thermal, and Piezoelectric Stress Components in $[45_3/-45_3]$ Plate Subject to 30°C Gradient with 185 Volts Applied on Upper and -105 Volts Applied on Lower Piezoceramic Actuators (a): σ_{xx}

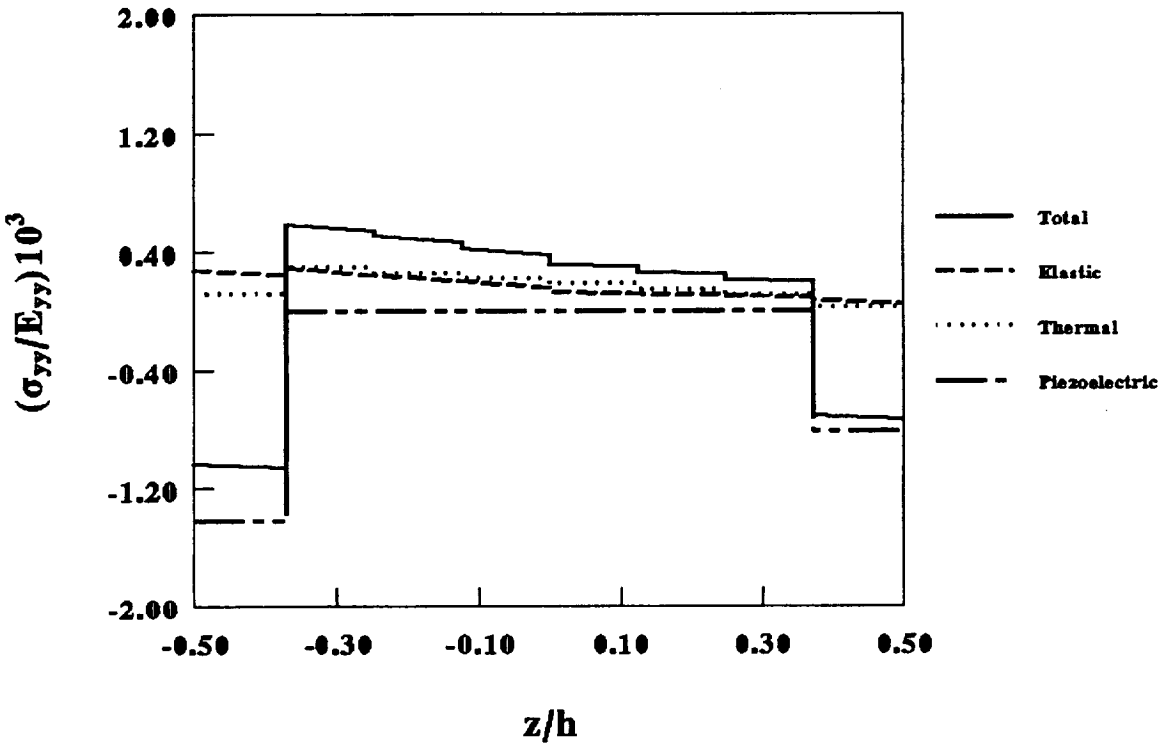

Figure 10: Elastic, Thermal, and Piezoelectric Stress Components in $[45_3/-45_3]$ Plate Subject to 30°C Gradient with 185 Volts Applied on Upper and -105 Volts Applied on Lower Piezoceramic Actuators (b): σ_{yy}

REPORT DOCUMENTATION PAGE

Form Approved
OMB No. 0704-0188

1. AGENCY USE ONLY (*Leave blank*)	2. REPORT DATE	3. REPORT TYPE AND DATES COVERED
	July 1996	Technical Memorandum

4. TITLE AND SUBTITLE

Layerwise Finite Elements for Smart Piezoceramic Composite Plates in Thermal Environments

5. FUNDING NUMBERS

WU-505-63-5B

6. AUTHOR(S)

Ho-Jun Lee and Dimitris A. Saravanos

7. PERFORMING ORGANIZATION NAME(S) AND ADDRESS(ES)

National Aeronautics and Space Administration
Lewis Research Center
Cleveland, Ohio 44135-3191

8. PERFORMING ORGANIZATION REPORT NUMBER

E-10290

9. SPONSORING/MONITORING AGENCY NAME(S) AND ADDRESS(ES)

National Aeronautics and Space Administration
Washington, D.C. 20546-0001

10. SPONSORING/MONITORING AGENCY REPORT NUMBER

NASA TM-106990
AIAA-96-1277

11. SUPPLEMENTARY NOTES

Prepared for the 37th Structures, Structural Dynamics, and Materials Conference and Exhibit cosponsored by AIAA, ASME, ASCE, AHS, and ASC, Salt Lake City, Utah, April 15-17, 1996. Ho-Jun Lee, NASA Lewis Research Center and Dimitris A. Saravanos, Ohio Aerospace Institute, 22800 Cedar Point Road, Cleveland, Ohio 44142 and Resident Research Associate at Lewis Research Center. Responsible person, Ho-Jun Lee, organization code 5210, (216) 433-3316.

12a. DISTRIBUTION/AVAILABILITY STATEMENT

Unclassified - Unlimited
Subject Category 24

This publication is available from the NASA Center for AeroSpace Information, (301) 621-0390.

12b. DISTRIBUTION CODE

13. ABSTRACT (*Maximum 200 words*)

Analytical formulations are presented which account for the coupled mechanical, electrical, and thermal response of piezoelectric composite laminates and plate structures. A layerwise theory is formulated with the inherent capability to explicitly model the active and sensory response of piezoelectric composite plates having arbitrary laminate configurations in thermal environments. Finite element equations are derived and implemented for a bilinear 4-noded plate element. Application cases demonstrate the capability to manage thermally induced bending and twisting deformations in symmetric and antisymmetric composite plates with piezoelectric actuators, and show the corresponding electrical response of distributed piezoelectric sensors. Finally, the resultant stresses in the thermal piezoelectric composite laminates are investigated.

14. SUBJECT TERMS

Actuators; Composite materials; Finite element method; Laminates; Piezoelectric ceramics; Piezoelectricity; Sensors; Smart structures

15. NUMBER OF PAGES

49

16. PRICE CODE

A03

17. SECURITY CLASSIFICATION OF REPORT	18. SECURITY CLASSIFICATION OF THIS PAGE	19. SECURITY CLASSIFICATION OF ABSTRACT	20. LIMITATION OF ABSTRACT
Unclassified	Unclassified	Unclassified	

National Aeronautics and
Space Administration

Lewis Research Center
21000 Brookpark Rd.
Cleveland, OH 44135-3191